UNIVERSITY OF MINNESOTA
ST. ANTHONY FALLS HYDRAULIC LABORATORY

Project Report No. 175

HEADLOSS CHARACTERISTICS OF SIX PROFILE-WIRE SCREEN PANELS

by

Heinz Stefan

and

Alec Fu

Prepared under contract with

Johnson Division UOP, Inc.
St. Paul, Minnesota

for

Consumer Power Company
Jackson, Michigan

and

Commonwealth Associates, Inc.
Jackson, Michigan

September, 1978
Minneapolis, Minnesota

University of Minnesota
St. Anthony Falls Hydraulic Laboratory

Project Report No. 175

HEADLOSS CHARACTERISTICS OF SIX PROFILE-WIRE SCREEN PANELS

by

Heinz Stefan

and

Alec Fu

Prepared under contract with

Johnson Division UOP, Inc.
St. Paul, Minnesota

for

Consumer Power Co.
Jackson, Michigan

and

Commonwealth Associates, Inc.
Jackson, Michigan

September 1978
Minneapolis, Minnesota

Screen Panels (15" x 24")
Wire Spacings are 3/8" (Screens No. 1. 3, 4, and 5),
1/2" (Screen No. 2) and 2 mm (Screen No. 6)

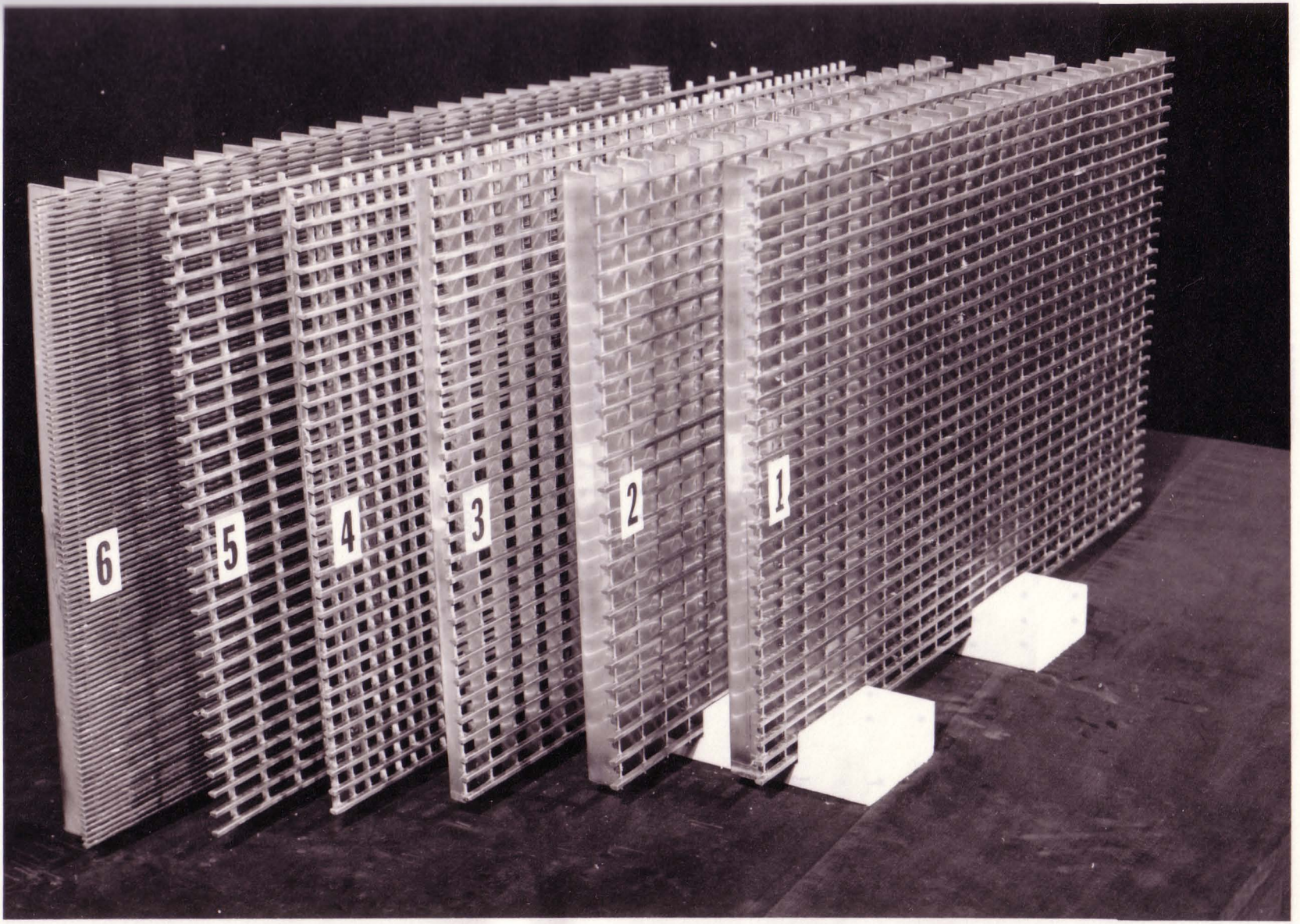
6
5
4
3
2
1

CONTENTS

ABSTRACT

Headloss coefficients for six screen panels manufactured by the Johnson Division UOP, Inc., Minnesota were determined experimentally. The screens are considered for use at the cooling water intake of Consumers Power Company's James H. Campbell Unit No. 3. The plant is located on the east shore of Lake Michigan near Grand Rapids, Michigan. The flat screen panels, 24 x 15 inches in size and of differing wire and rod assembly, were tested in a laboratory flume at approach velocities ranging from 0.9 to 2.6 ft/sec. The angle of approach relative to the screen surface was varied from 90° to 45° in intervals of 15°. In the range of velocities and angles tested the headlosses were found to be less than 0.3 ft of water. Headloss coefficients (using approach velocity head as a reference) ranged from 0.5 to 2.8 at 90° angle of approach. The experimental data led to the conclusion that the screens tested would not produce an appreciable headloss when used in low velocity surface water intakes.

Listing of Studies

for the James H. Campbell

Unit No. 3 Cooling Water Intake

1. H. Stefan and A. Fu, "Headloss Characteristics of Six Profile-Wire Screen Panels," University of Minnesota, St. Anthony Falls Hydraulic Laboratory, Minneapolis, Minnesota, Project Report No. 175, September 1978, 71 pages.

2. H. Stefan and A. Fu, "Collector Well Study for the Cooling Water Intake System of the James H. Campbell Electric Power Generating Plant, Unit No. 3," University of Minnesota, St. Anthony Falls Hydraulic Laboratory, Minneapolis, Minnesota, Project Report No. 176, November 1978, 46 pages.

3. H. Stefan, W. Q. Dahlin, J. F. Ripken, A. Wood, and T. Winterstein, "Experimental Flow Studies with the Dual-Screen Cooling Water Intake Assembly ("Riser") for the James H. Campbell Electric Power Generating Plant, Unit No. 3," University of Minnesota, St. Anthony Falls Hydraulic Laboratory, Project Report No. 177, December 1978, 130 pages.

4. H. Stefan, C. Shanmugham, and S. Dhamotharan, "Cooling Water Manifold Intake (Header) Study for the James H. Campbell Electric Power Generating Plant, Unit No. 3," University of Minnesota, St. Anthony Falls Hydraulic Laboratory, Minneapolis, Minnesota, Project Report No. 178, January 1979, 59 pages.

5. John M. Killen and H. Stefan, "Hydraulic Analysis of Alternative Cooling Water Intake Designs for the James H. Campbell Electric Power Generating Plant, Unit No. 3," University of Minnesota, St. Anthony Falls Hydraulic Laboratory, Minneapolis, Minnesota, External Memorandum No. 161, December 1978, 22 pages.

LIST OF FIGURES

LIST OF FIGURES (cont'd)

LIST OF FIGURES (cont'd)

LIST OF TABLES

HEADLOSS CHARACTERISTICS OF SIX SCREEN PANELS

I. Introduction

Screens are used in surface water intakes to prevent entrainment of debris and aquatic life when supplying cooling water to power generating plants. At high intake velocities, screens may cause injury or death to aquatic life, particularly fish. At elevated velocities, small fish may be entrained and fish too large to pass through the opening slots may be impinged on the screen surface. Design for low withdrawal velocities and use of fine mesh screens are expected to minimize both entrainment and impingement conditions.

A screen may be defined as a regular assemblage of elements forming a pervious sheet which is relatively thin in the direction of flow. Examples are woven round-wire screens, perforated thin sheets, grids of bars of rectangular cross section, screens composed of streamlined wire, etc. A screen is characterized geometrically by element type (round-wire, etc.), by element arrangement (square mesh, etc.), and by screen shape (plane, etc).

The losses in surface intake screens are determined by screen geometry, scale effects (Reynolds number), and the orientation of the screen with respect to the flow direction.

This report describes experiments and associated analysis to determine the headloss characteristics of welded profile wire fine-meshed 3/8", 1/2" and 2 mm slot opening screens over a range of flow velocities. The headloss coefficients of six screens of different geometry at various orientations with respect to the flow direction were determined.

The screens described herein are manufactured by Johnson Divison UOP Inc, St. Paul, Minnesota. The study was conducted under contract with Johnson Division for Consumer Power Company and for Commonwealth Associates, Inc., both in Jackson, Michigan.

II. Description of Screen Panels

A schematic view showing the general features of the six screen panels tested is given in Fig. 1. The dimensions identified by letters 'a' through 'e', 'r', and 'w' in Fig. 1 are specified in Table 1.

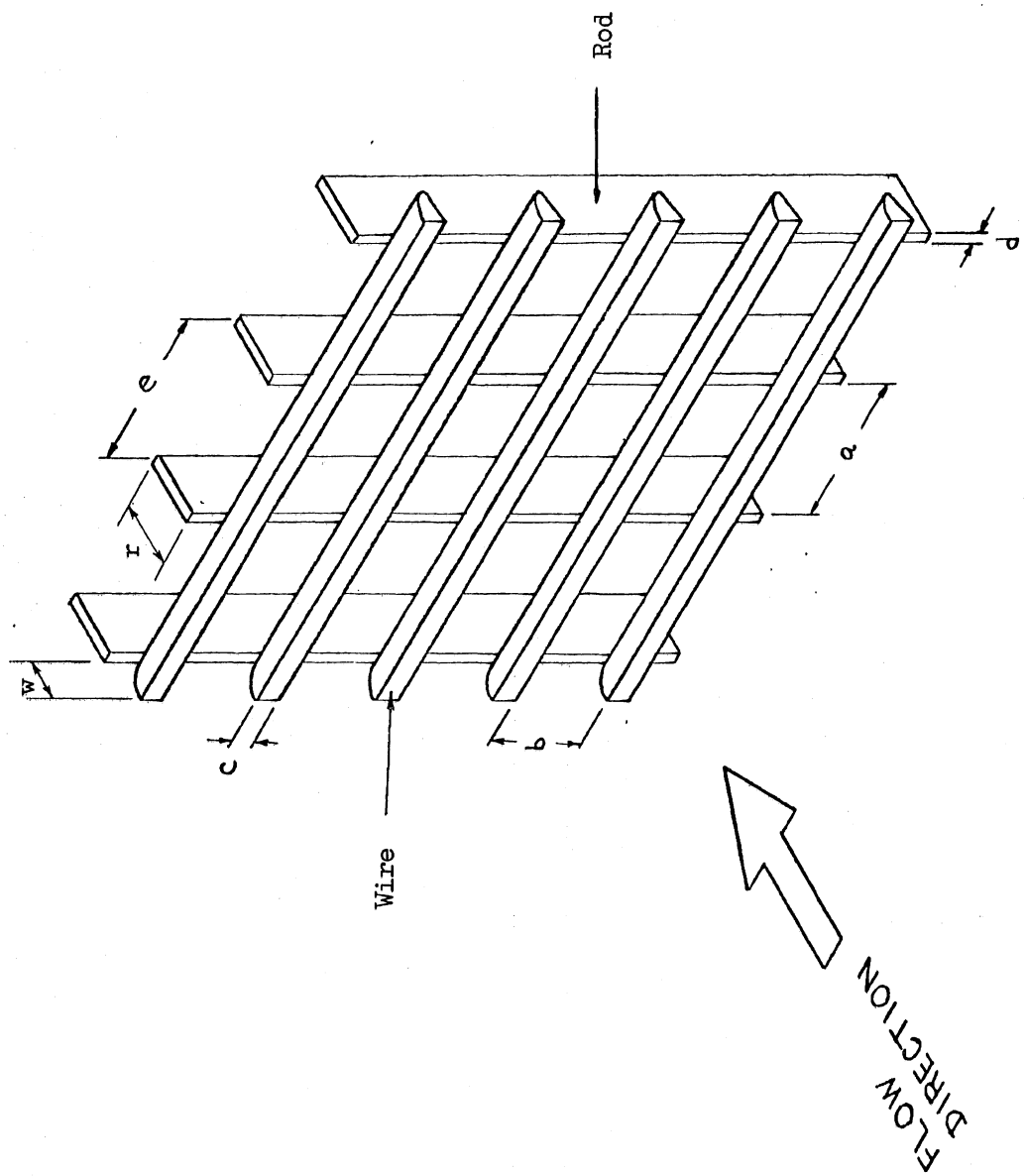

Figure 1. Schematic View of Screen Panel

TABLE 1. Dimensions of Screen Panels*

Screen Panel Number	Open Spacing		Widths		Rod Center Spacing	Lengths		Per cent** open area
	Rods (a)	Wires (b)	Wire (c)	Rod (d)	(e)	Rod (r)	Wire (w)	
1	.930"(15/16" approx.)	3/8"(.375")	.128"	.070"	1"	1"	1/4"	74.5
2	.930"(15/16" approx.)	1/2"(.500")	.128"	.070"	1"	1"	1/4"	79.6
3	.930"(15/16" approx.)	3/8"(.375")	.128"	.070"	1"	1/2"	1/4"	74.5
4	.348(5/16"-3/8")	3/8"(.375")	.128"	.152"	1/2"	3/16"	1/4"	74.5
5	.848(13/16"-7/8")	3/8"(.375")	.128"	.152"	1"	3/16"	1/4"	74.5
6	.930(15/16" approx.)	2mm (.079")	.075"	.070"	1"	1"	3/16"	51.3

* specified by Johnson Division UOP.

** $\frac{b}{b+c}$, rods not taken into consideration.

The screens are made of stainless steel and welded at all crossings of the profile wire and the rods.

The profiles of wires and rods used for all six screens are given in Fig. 2. The wires for screens 1 through 5 were identical in shape. The rods for screens 1, 2, and 3 were rectangular but differed in length.

III. Literature Review on Headloss Coefficients of Screens

Headloss coefficients of the type of screens being tested could not be found in the literature. Most of the available literature deals with screens made of round wires and with woven screens.

The flow through a screen can be considered as flow through a number of orifices or nozzles in parallel (see e.g. Ref. 1).* The headloss across a screen is often expressed in terms of a headloss coefficient and the velocity head just upstream of the screen. The headloss coefficient is a function of the open area fraction of a screen and a dimensionless discharge coefficient which is a function of Reynolds number. The Reynolds number can be based on aperture width, upstream velocity and the fractional free projected area of screen. For plain rectangular mesh screens, a plot of discharge coefficients versus Reynolds numbers is given in Reference 1.

For closed conduit flow and for screens made of circular metal wire, Idel'Chik (Ref. 2) expressed the Reynolds number in terms of the wire diameter and the upstream velocity. The headloss coefficient was expressed as the ratio of headloss to upstream velocity head. The loss coefficient was related to the ratio of open flow area in the screen to the area of the cross-section before the obstruction. At $Re \geq 400$, the loss coefficient could be determined from a simple mathematical expression. At $Re < 400$, a correction factor given in a graph in Ref. (2) had to be used.

In a manual published by the British Hydromechanics Research Association (Ref. 3), a solidity factor was defined as the ratio of the area occupied by bars to the total cross-sectional area. The Reynolds number was calculated using mean approach velocity, wire or bar diameter and the solidity factor in accounting for the obstruction. For a woven round-wire screen and round-bar screen, and for Reynolds numbers greater than 300,

*Biographical references are given on page 71.

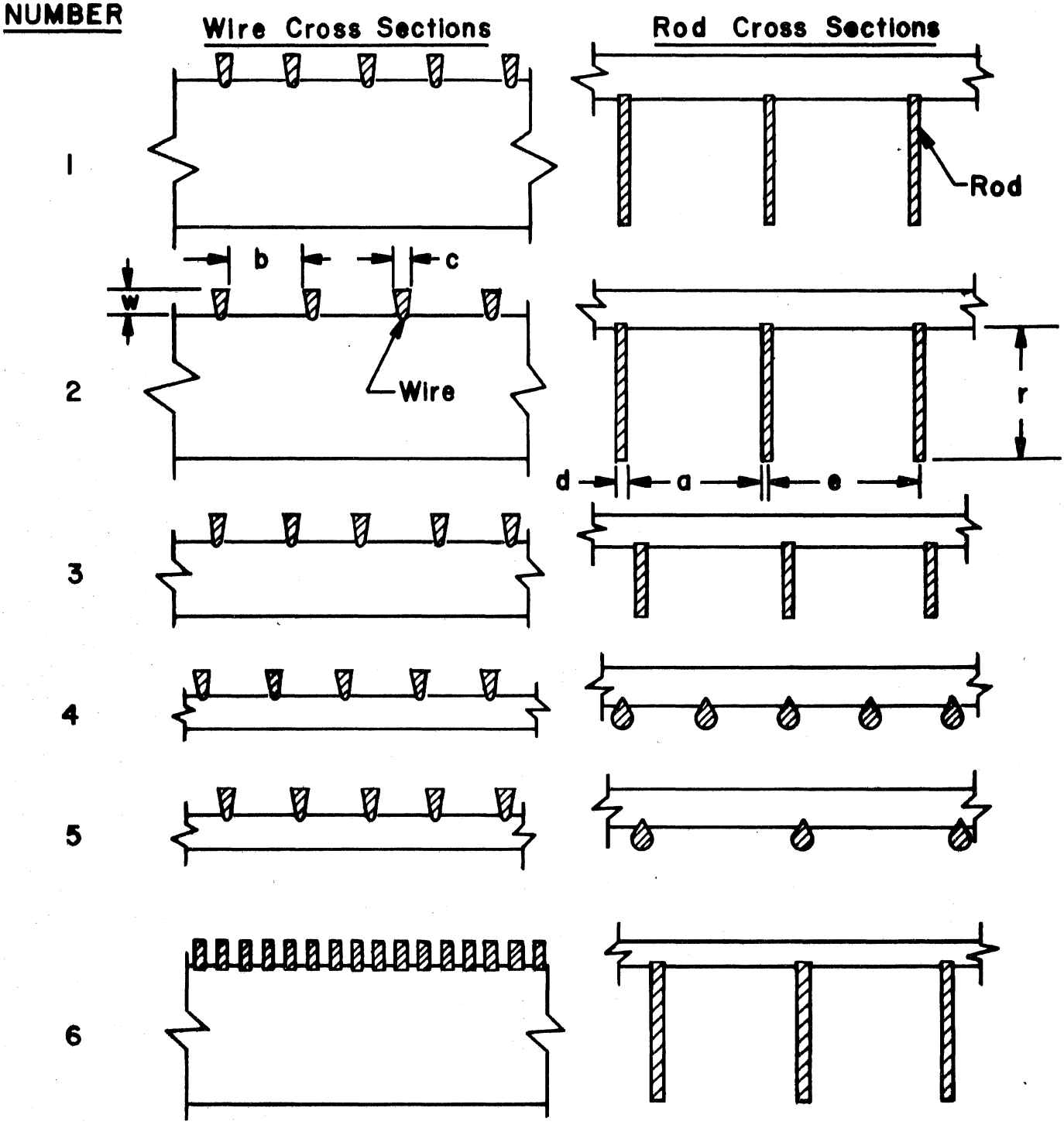

Figure 2 PROFILES OF WIRES AND RODS
(APPROXIMATE FULL SCALE)
SEE TABLE I for actual dimensions of
a, b, c, d, e, r, and w

the headloss coefficient was solely a function of solidity factor. It was indicated that if the thickness of the bars in the stream direction was greater than half the gap between the bars, flow re-attachment would occur and loss coefficients would be reduced. By using streamlined bars, loss coefficients might be halved.

In the case of duct flow, Monson and McDonald (Ref. 4) obtained an expression for the loss coefficient by first determining the drag on the front and rear rods and then converting the drag to loss coefficients. The loss coefficient is a measure of total pressure loss across the screen.

For woven screens, Monson and McDonald made use of the approach velocity, wire diameter, and open area fraction to calculate the Reynolds number of the wire. The loss coefficient was related to open area fraction (a function of wire diameter and orthogonal bar spacings) and the drag coefficient on the Reynolds number of the wire.

For cross-bar matrices screens, Monson and McDonald (Ref. 4) used the approach velocity and the hydraulic diameter of the opening in calculating the Reynolds numbers. The loss coefficient was related to open area fraction of the front row, the drag coefficients of front rods and rear rods. In determining the drag coefficients, the effective Reynolds number of front rods (in terms of approach velocity, front rod diameter and open area fraction of front row) and the effective Reynolds number of rear rods (in terms of approach velocity, rear rod diameter and open area fraction) were used. The corresponding drag coefficients were read from graphs prepared by Cornell (Ref. 5).

Wieghardt (Ref. 6), as quoted in Ref. 5, visualized the flow through round-wire screen as similar to the flow over single infinite cylinders bathed in a uniform flow of velocity $V_1(1 - S)$, due to the constriction imposed by the screen. V_1 was the upstream velocity and S the ratio of blocked area to total area. He expressed the loss coefficient (λ) as the ratio of total pressure loss in a screen (Δp_T) to the upstream dynamic pressure ($\frac{1}{2}\rho V_1^2$). Thus Wieghardt correlated $\lambda(1 - S)^2/S$ with $Re = V_1 d(1 - S)\nu$, anticipating a curve similar in trend to the drag coefficient. d was the diameter of the round wire. Wieghardt's correlation covered the range $60 < Re < 1{,}000$ and is represented by the relation

$$\lambda (1 - S)^2/S = 6(Re)^{-\frac{1}{2}} \tag{1}$$

MacDougall (Ref. 4) correlated data in the range $0.006 < Re < 20$ and obtained the relation

$$\lambda = \frac{33.93}{Re} \frac{S(1 - S)^{-1.27}}{1 + (1 - S)^{\frac{1}{2}}} \tag{2}$$

For low Mach number flow normal to plane sharp-edged screens, Weinig[1] used a two dimensional model of the flow around one-half of a screen element for the flow in ribbon parachutes and compared the results successfully with experimental data for losses in strip screens. The loss coefficient was given by

$$\lambda = \left[1 - C_c (1 - S)\right]^2 \Big/ \left[C_c^2 (1 - S)^2\right] \tag{3}$$

under the assumption of incompressible, perfect fluid flow, the wake velocity being taken as zero. Weinig used the theoretical results of Von Mises for contraction coefficient C_c, based on a free streamline potential theory model of flow in a sharp edged orifice.

IV. Experimental Apparatus

Experiments were conducted in a 50 ft long glass walled laboratory flume of 24" width and 15" depth. The screen panels were also 24" x 15". The water level in the channel could be controlled by an adjustable gate at the downstream end of the channel (Fig. 3). Water from the Mississippi river was fed into the headbox of the channel through a 12" line in which an orifice flow meter is installed. A calibration curve for the flow meter was prepared prior to the screen panel experiments. The laboratory weighing tanks were used for the calibration.

The screen panels were installed in the flume at a distance of about 15 ft from the upstream gate. Disturbances from the upstream gate and from the header box were quite small at that distance.

Travelling point-gauges were installed upstream and downstream from the screen panel to measure water surface elevations.

---

[1] Quoted in Ref. (5).

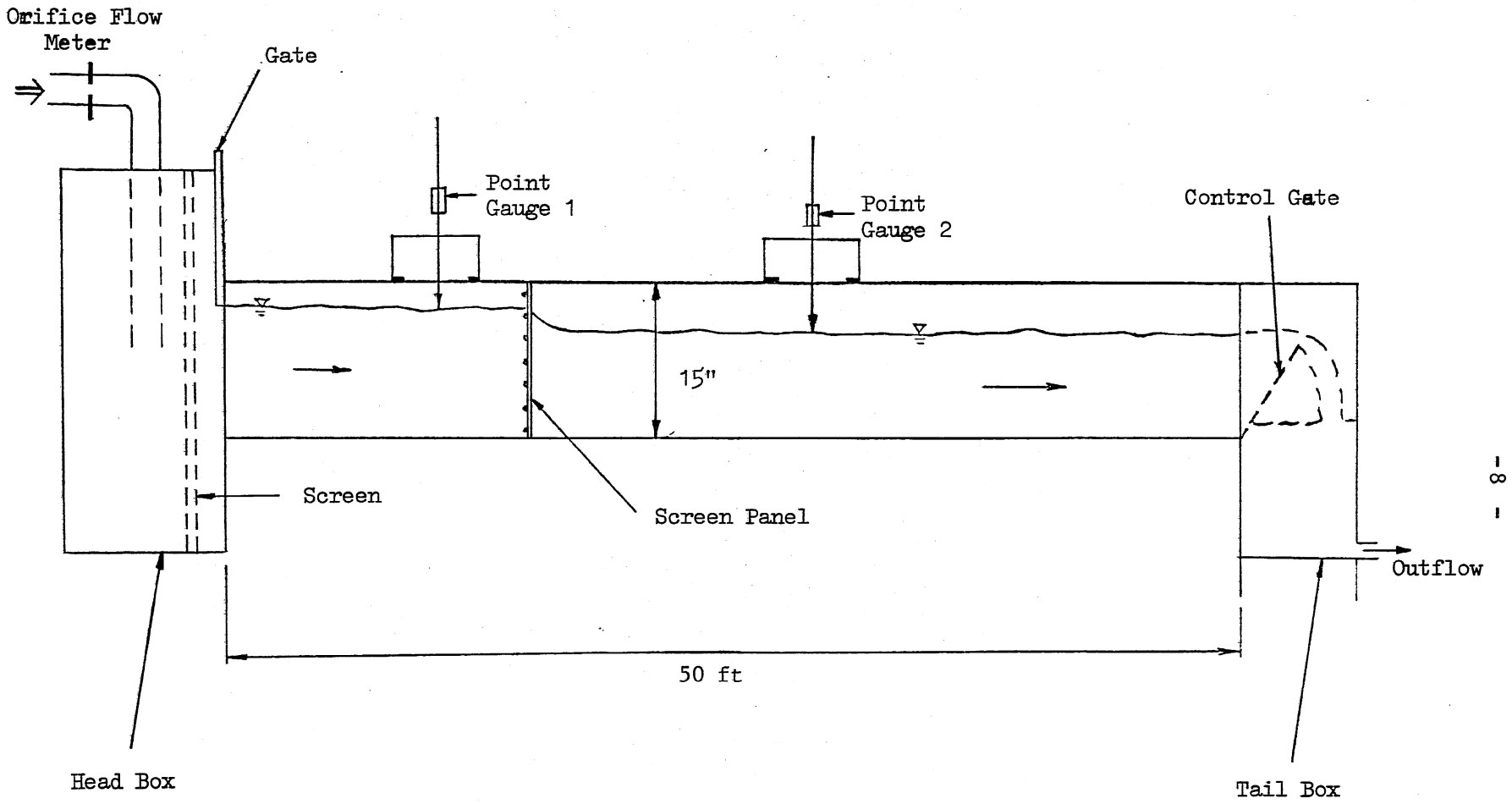

Fig. 3 - 50-ft Glass-Walled Flume (Schematic).

The orientation of a screen panel relative to the channel axis was variable. Six different orientations were investigated, as shown in Fig. 4.

Flow in the channel was maintained at subcritical conditions at all times. The upstream depth was maintained at 12-1/2" for all runs except $\alpha = 45^{\circ}$, when a depth of 9" had to be maintained, because of the limited height of the panel in the tilted position.

Standing waves were generated downstream from the screen panel. At high discharges the amplitudes of the waves were large enough to induce significant errors in measurements. As a remedy, a wooden board was placed on the water surface at a distance of about one foot downstream from the screen panel. The board was taken out whenever the standing waves were insignificant.

Rather than manufacturing panels of different length, a contraction was installed in the channel to fill the gap between the end of the screen panel and the sidewall when the angle β was different from 90°, as shown in Fig. 4c. The shape of the contractions used is shown in Fig. 5. Each was 15" high (equal to the maximum depth of the flume).

Photographs of several installed screens are shown in Fig. 6 and Fig. 7.

V. Experimental Procedures

The following procedure was followed in the experiments.

(1) Install desired screen panel at proper angle.

(2) Set maximum discharge through channel.

(3) Adjust control gate at downstream end to maintain subcritical flow in channel and to keep water depth upstream from screen panel at 12½". Decrease discharge, if necessary, until subcritical flow is achieved downstream from the screen panel.

(4) Secure board on downstream water surface at a distance of about one foot from the screen panel to suppress any possible standing waves generated. Take out the board whenever the waves and surface disturbance created by the screen becomes insignificant.

(5) Read manometer deflection of orifice meter and determine the corresponding discharge from the calibration curve.

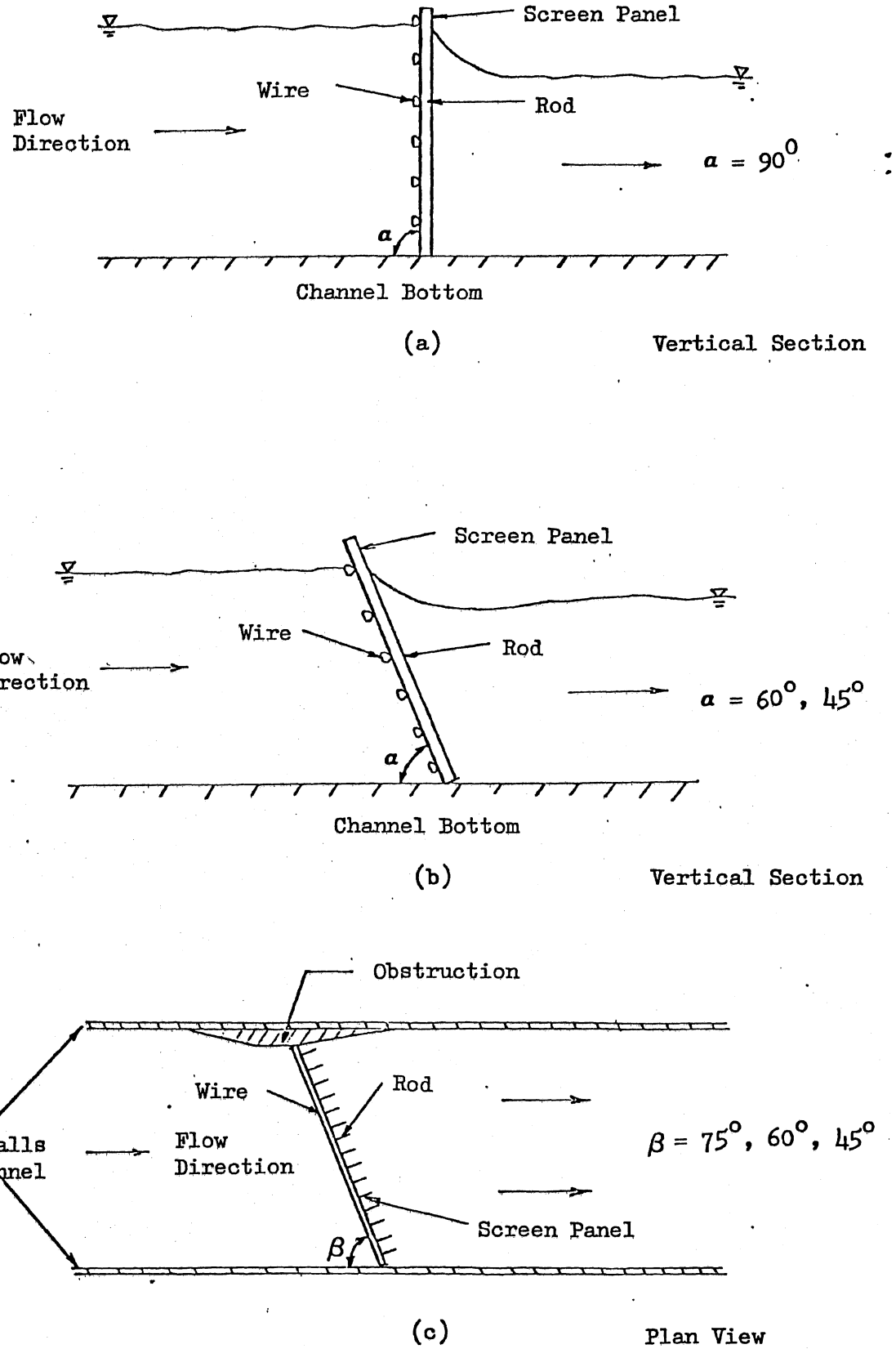

Fig. 4 - Screen Panels Oriented at α and β Angles in Flume.

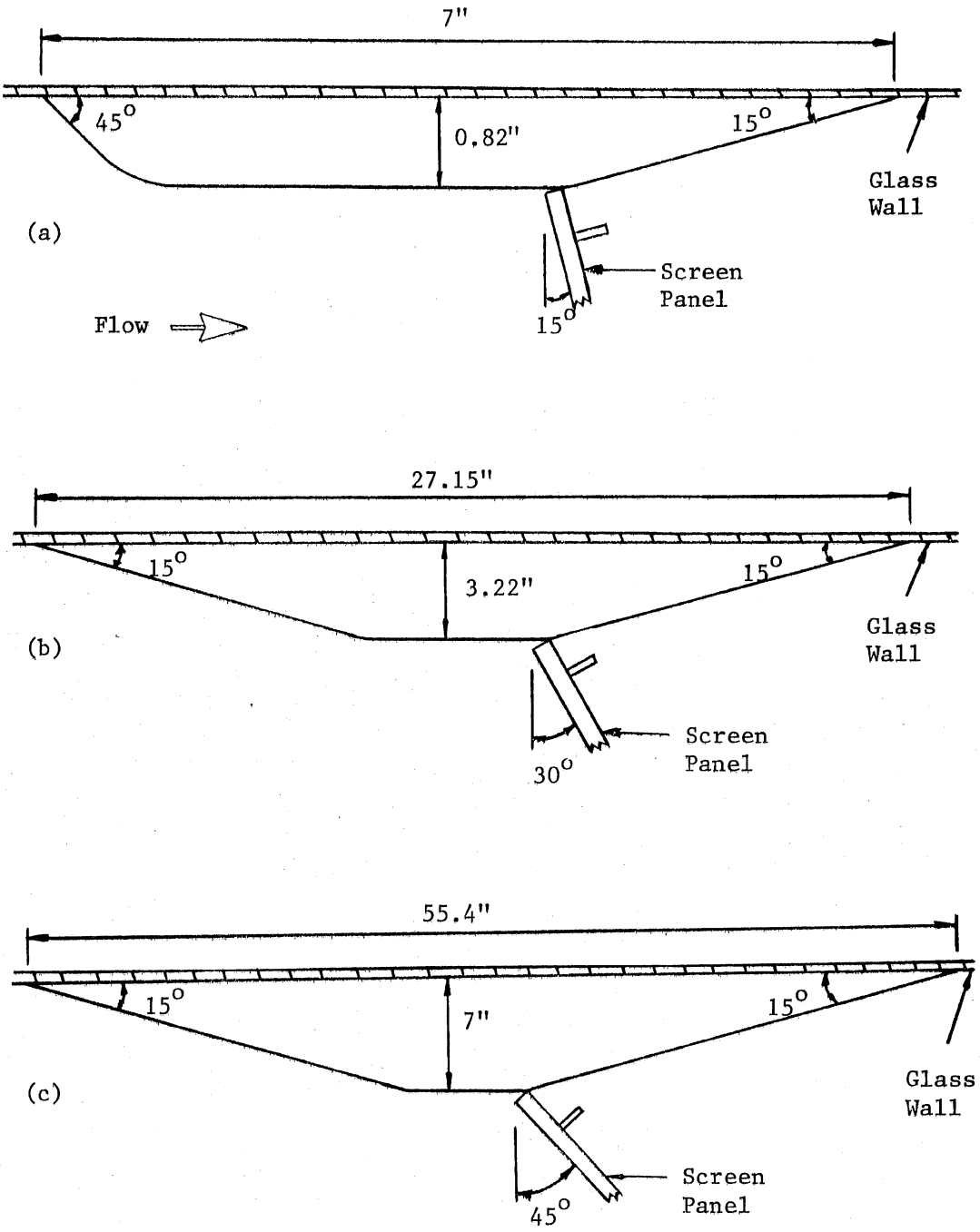

Fig. 5 - Contractions Used for Different Screen Angles β.
(a) $\beta = 75^{o}$, (b) $\beta = 60^{o}$, (c) $\beta = 45^{o}$

Screen No. 1, $\beta = 90^{\circ}$, $\alpha = 90^{\circ}$.

Side View

Screen No. 1, $\beta = 90^{\circ}$, $\alpha = 90^{\circ}$.

Overhead View

Fig. 6(a) - Screen Installation in Laboratory Flume.

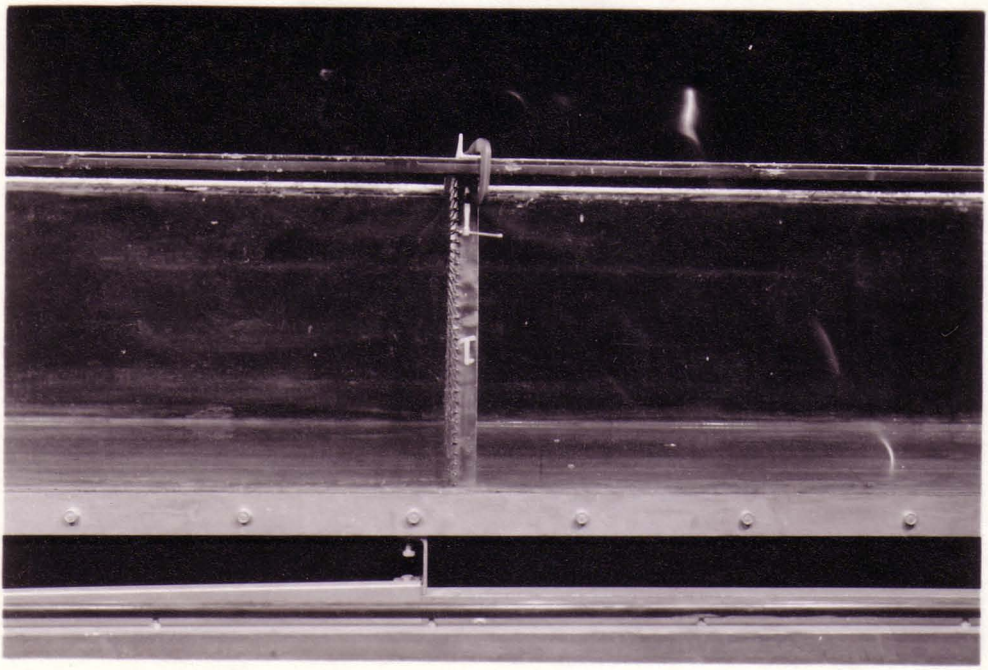

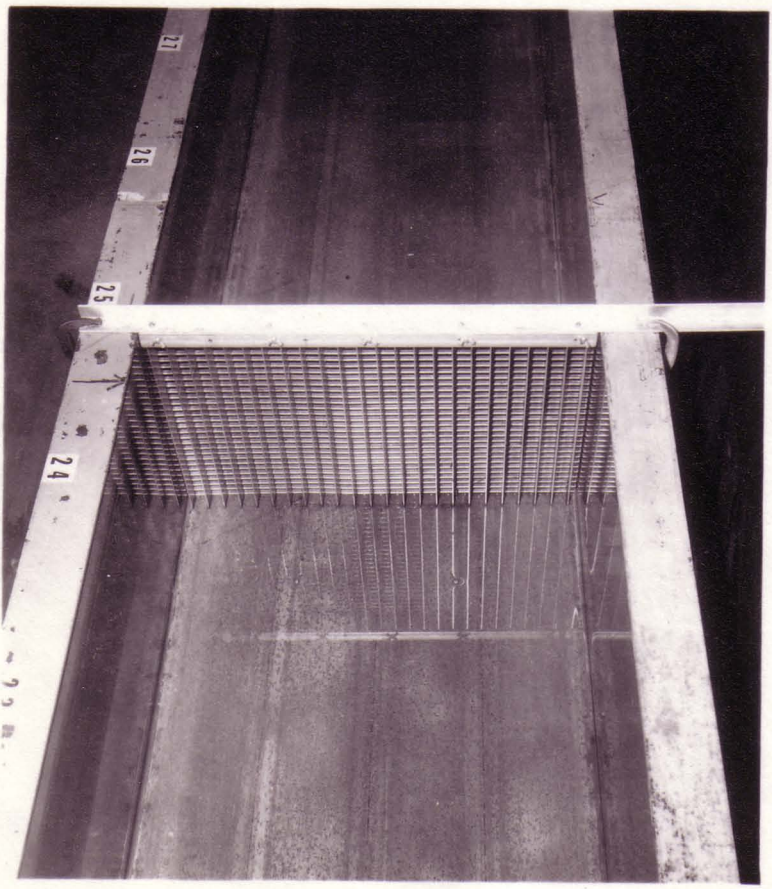
27
26
25
24

Screen No. 1, $\beta = 90^{\circ}$, $\alpha = 60^{\circ}$.
Side View

Screen No. 1, $\beta = 90^{\circ}$, $\alpha = 60^{\circ}$.
Overhead View

Fig. 6(b) - Screen Installation in Laboratory Flume.

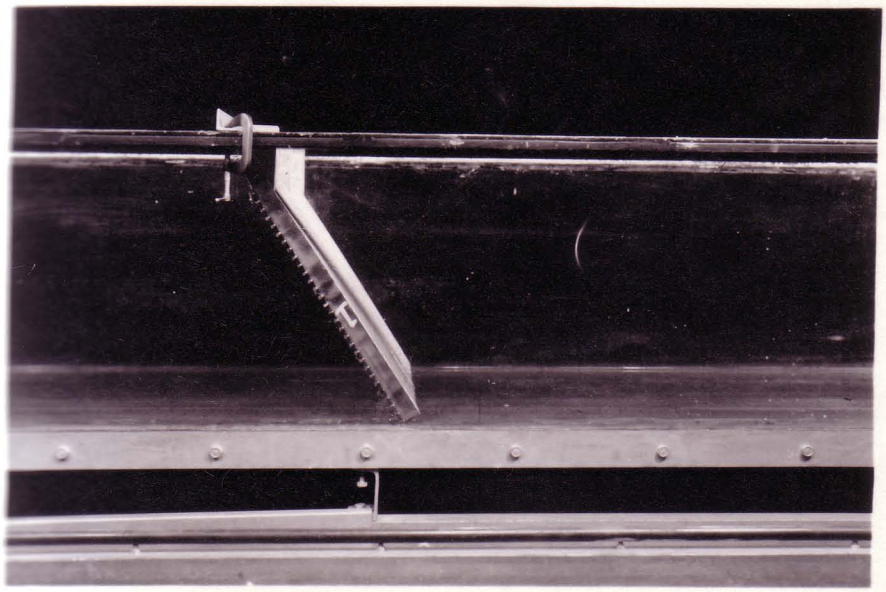

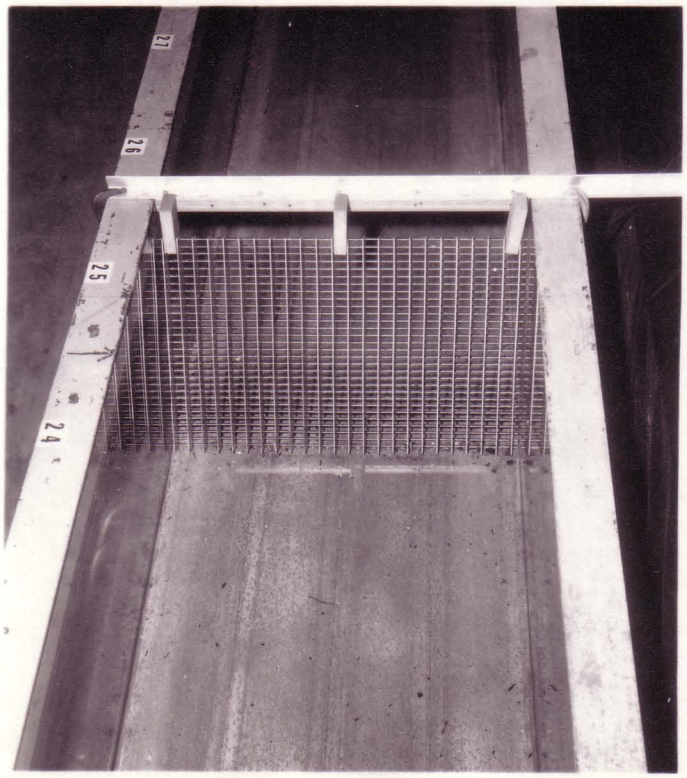
27
26
25
24

Screen No. 4, $\beta = 45^{\circ}$, $\alpha = 90^{\circ}$
Side View

Screen No. 4, $\beta = 45^{\circ}$, $\alpha = 90^{\circ}$
Overhead View

Fig. 6(c) - Screen Installation in Laboratory Flume.

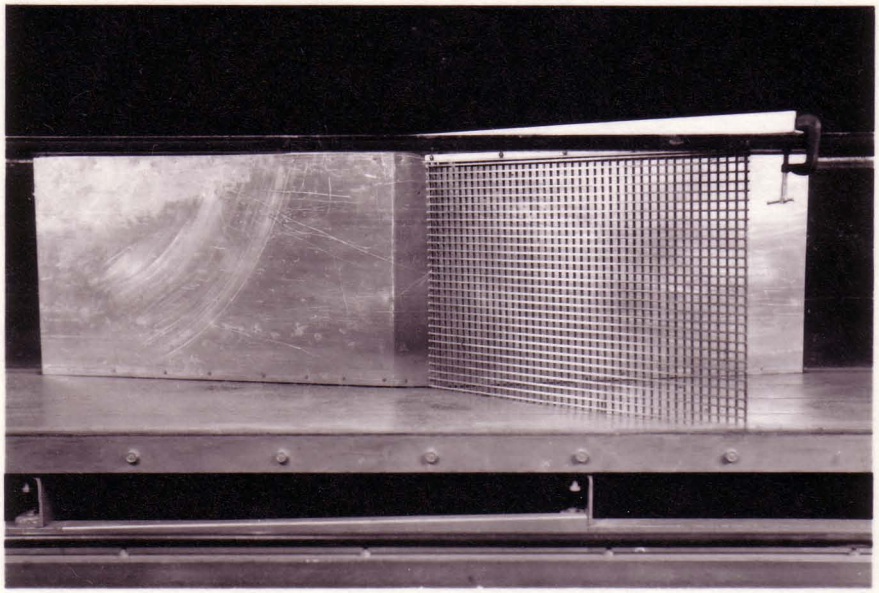

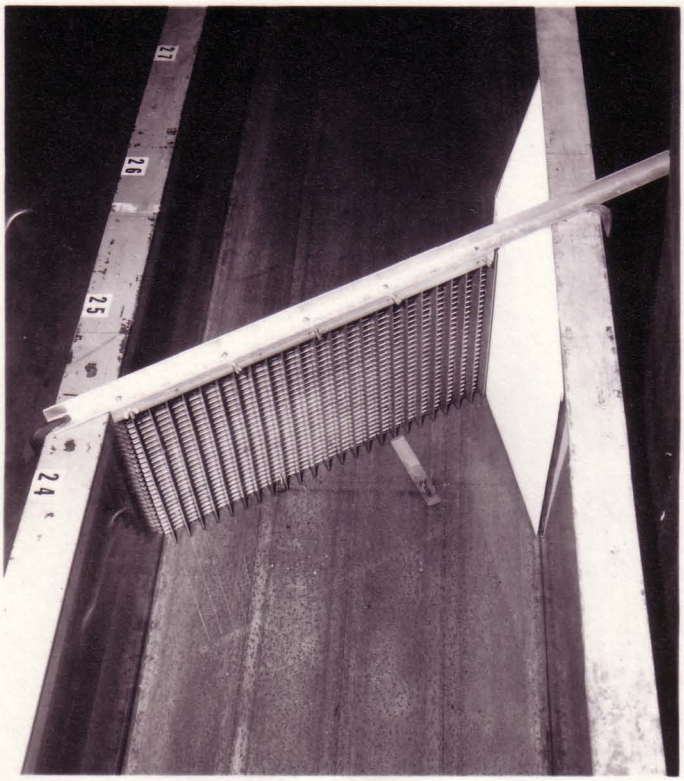
27
26
25
24

Screen No. 1, $\beta = 90^{\circ}$, $\alpha = 60^{\circ}$
Side View

Screen No. 1, $\beta = 60^{\circ}$, $\alpha = 90^{\circ}$
Overhead view

Fig. 7 - Flow Through Screens.

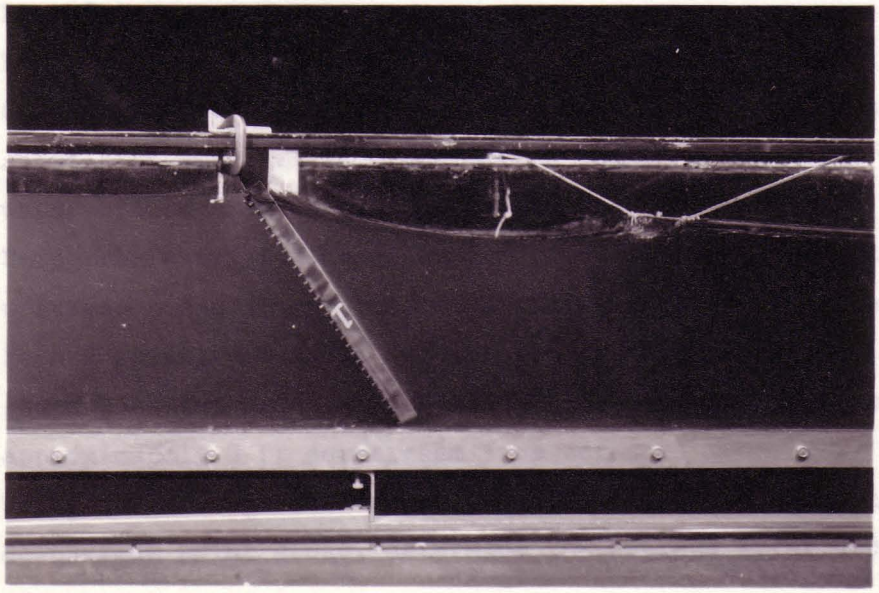

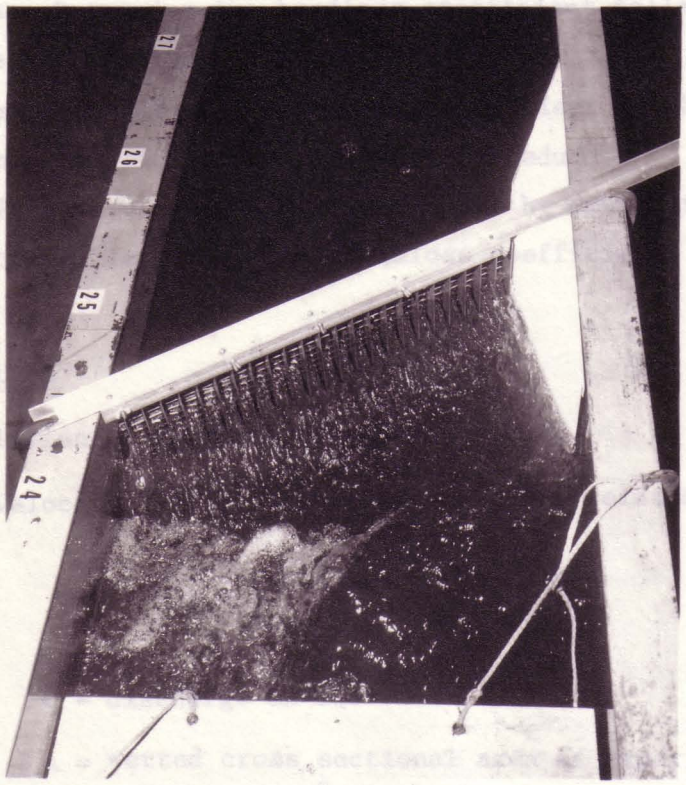
27
26
25
24

(6) Record water temperature.

(7) Record upstream water surface levels at five locations, each 6" apart, with the travelling point gauge 1. Start measurement about 4 ft upstream from the screen panel to avoid any back-water effect created by the screen.

(8) Using the average channel bottom elevation with respect to the upstream point gauge, determine the average water depth upstream.

(9) Record downstream water surface levels with the travelling point gauge 2 at ten locations, each 6" apart. Start measurement at approximately 3 ft downstream from screen.

(10) Using the average channel bottom elevation with respect to the downstream point gauge, determine the average water depth down-stream.

(11) Repeat (1) through (10) for smaller and smaller discharges until the water surface level drop at the screen is no longer detectable.

(12) Repeat (1) through (11) for a different screen.

(13) Repeat (1) through (12) for a different orientation of screen panels. Determine the headloss coefficient following the pro-cedure outlined in the next section.

(14) Determine headloss and headloss coefficient of channel without screen panel, following the above procedure.

(15) Calculate screen headloss coefficient by subtracting channel loss coefficient from bulk headloss coefficient.

VI. Data Reduction

(1) Calculation of average reference velocity

Velocity (V) is calculated using the relationship

$$V = \frac{Q}{A} \tag{4}$$

where Q = discharge in cfs

A = wetted cross sectional area of experimental channel in ft^2.

(2) Calculation of Reynolds number

Reynolds number (Re) is calculated using the relationship

$$Re = \frac{V\sqrt{ab}}{\nu} \tag{5}$$

where a,b = dimensions of opening of a grid in ft

ν = kinematic viscosity in $ft^2/sec.$

(3) Calculation of headloss coefficient

Writing the energy equation for an upstream and a downstream cross-section, we have

$$\frac{V_1^2}{2g} + y_1 = \frac{V_2^2}{2g} + y_2 + h_L \tag{6}$$

where V_1, V_2 = average velocities upstream and downstream from screen, respectively,

y_1, y_2 = average depths upstream and downstream from screen, respectively,

h_L = friction loss due to screen, channel walls and obstruction, if applicable.

Rearranging the above equation, we have

$$h_L = \frac{1}{2g}(V_1^2 - V_2^2) + (y_1 - y_2) \tag{7}$$

The headloss coefficient is expressed as the ratio of headloss to upstream velocity head, i.e. $K = h_L(V_1^2/2g)^{-1}$.

Headloss coefficients to account for the friction loss in the channel, the wave suppressing board, and the constriction were determined separately and are shown in Figs. 8a to 8d. The friction loss due to the obstruction at $\beta = 75^\circ$ was found to be almost undetectable. For practical purposes, the same calibration curve (Fig. 8a) has been used for cases at $\alpha = 90^\circ$ and $\beta = 75^\circ$. In Figs. 8a to 8d the coefficient increases as discharge decreases. (The one and only deviation is shown in Fig. 8c and is attributed to increased surface wave formation and the impact of the flow downstream from the contraction on the channel walls.) This indicates the presence of a Reynolds number effect and agrees with the findings of Cornell (Ref. 5) who stated

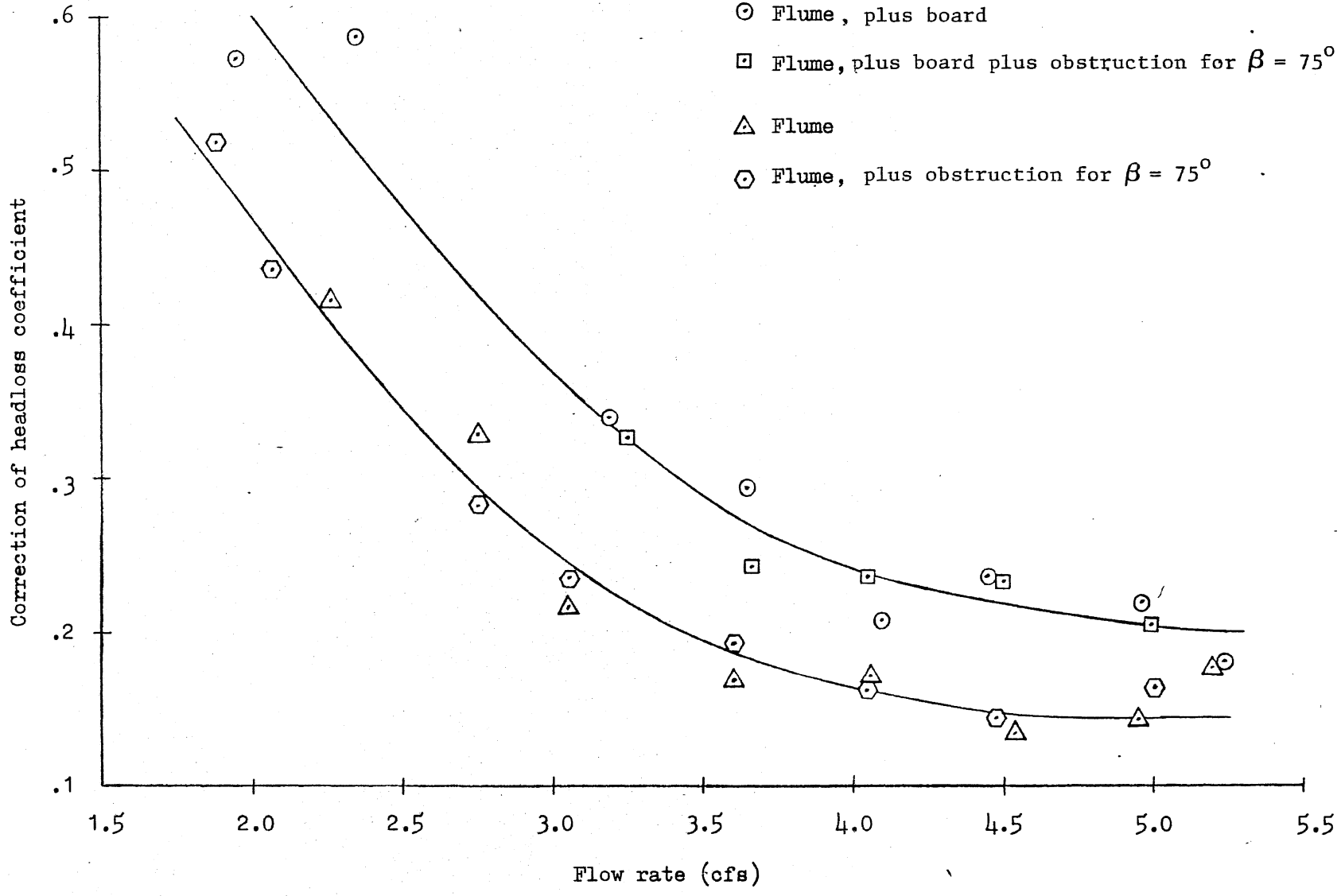

Fig. 8(a) - Headloss coefficient correction - 12.5" water depth.

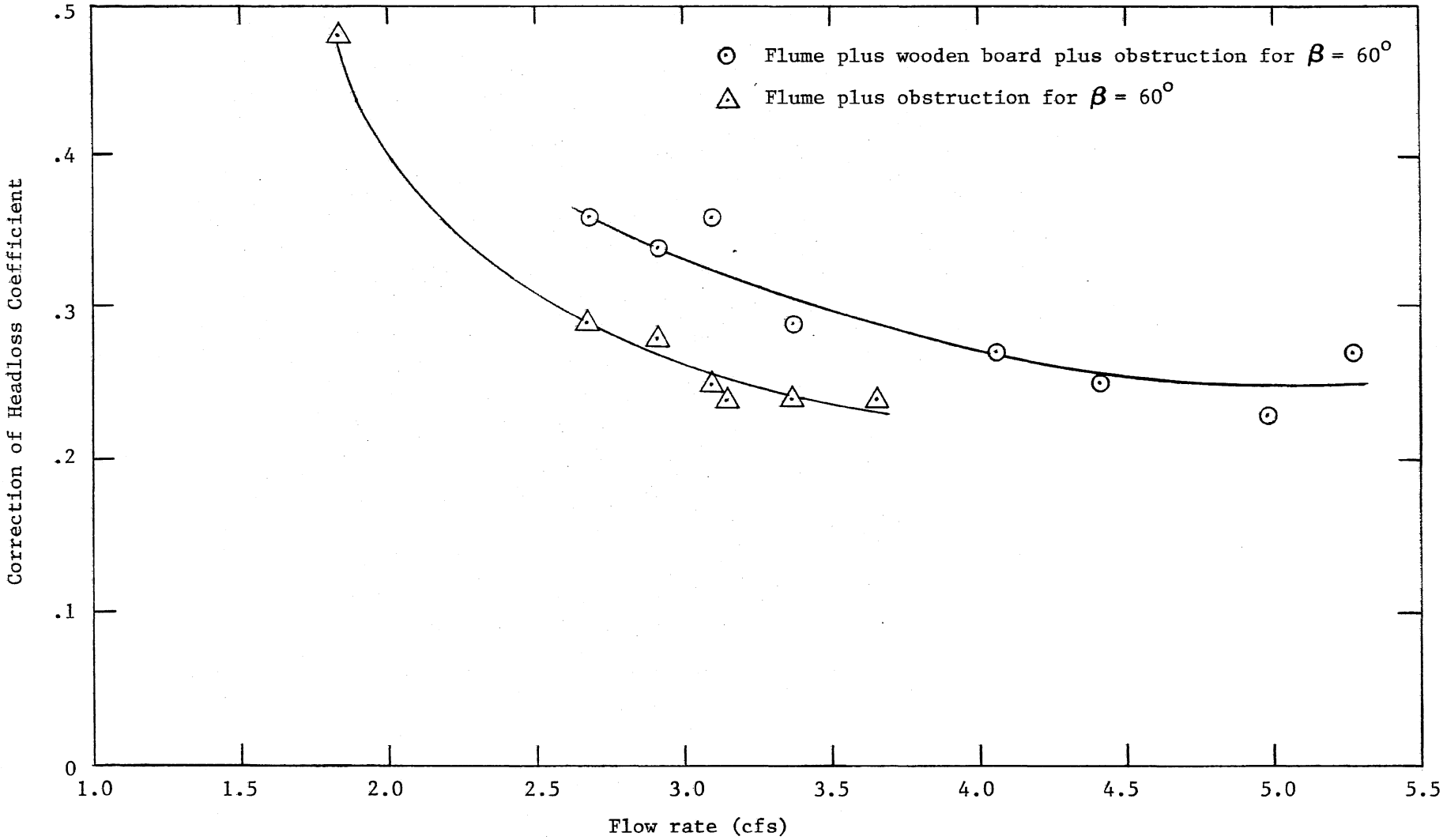

Fig. 8(b) - Headloss coefficient correction - 12.5" water depth.

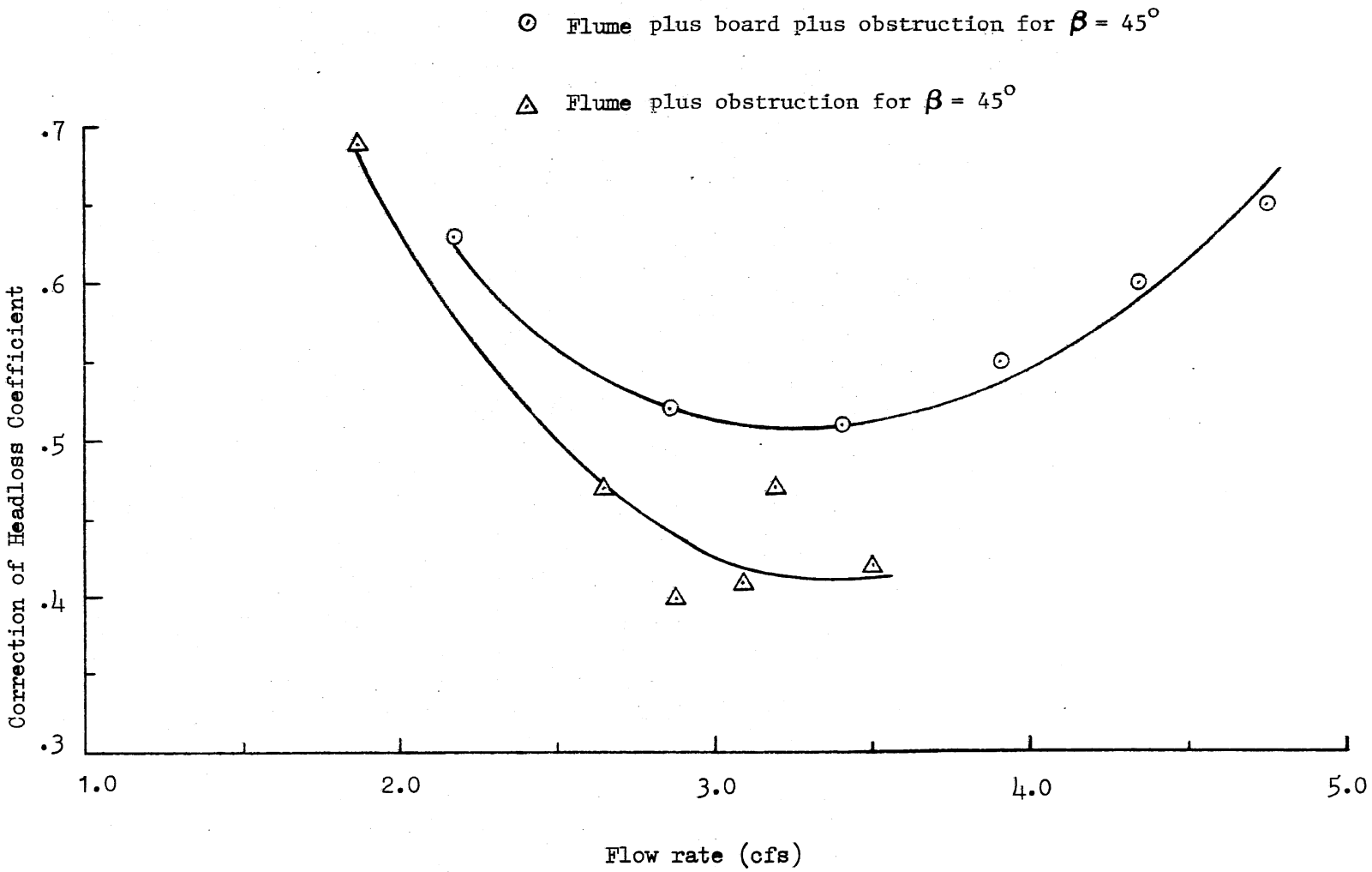

Fig. 8(c) : - Headloss coefficient correction - 12.5" water depth.

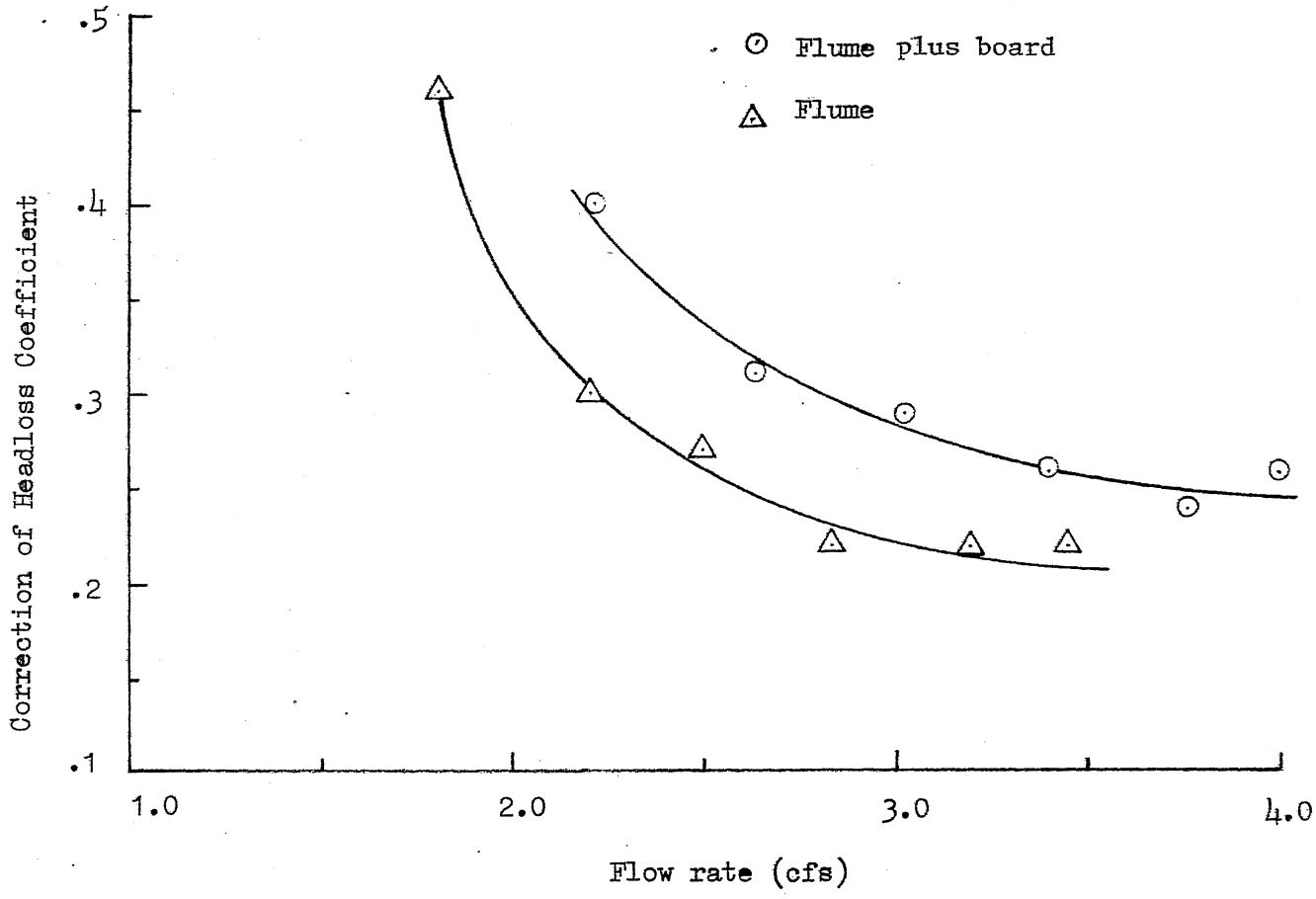

Fig. 8(d) - Headloss coefficient correction - 9.5" water depth.

"The effect of Reynolds number on loss is found to be small, except at very low Reynolds number". The headloss coefficient of the screen is obtained by subtracting the correction due to the flume (the board and the obstruction, where applicable) from the bulk headloss coefficient.

VII. Experimental Screen Headloss

Headloss coefficients determined for individual screens have been plotted vs. Reynolds number (defined by Eq. 5) in Fig. 9 (for $\alpha = 90^{\circ}$), Fig. 10 (for $\alpha = 75^{\circ}$), Fig. 11 ($\alpha = 60^{\circ}$), Fig. 12 ($\alpha = 45^{\circ}$), Fig. 13 ($\beta = 75^{\circ}$), Fig. 14 ($\beta = 60^{\circ}$), and Fig. 15 ($\beta = 45^{\circ}$).

Upon comparing the results shown in Figs. 9 thru 12, i.e. for cases with $\alpha = 90^{\circ}$, $\alpha = 75^{\circ}$, $\alpha = 60^{\circ}$, and $\alpha = 45^{\circ}$, it can be concluded (i) that the value of the loss coefficient k at the same Reynolds number increases as the angle of approach α decreases, and (ii) that the loss coefficient increases as the open area fraction of the screen decreases. Both results can be explained by the fact that headloss is directly proportional to the blocked area imposed, as will be shown in the next section.

For flow perpendicular to the screen, headloss coefficients for screens No. 1, 3, and 5 can practically be represented by the same curve. This is to be expected since the three screens have identical opening sizes and the same shapes of wires and rods. If a screen is tilted at an angle β, the length of the rod begins to play an important role. In Fig. 13, it can be seen that only the headloss coefficients of screens No. 3 and 5 (but not No. 1) can be represented by the same curve. Screen No. 1 has a longer rod than screens No. 3 and No. 5 and is therefore more effective in deflecting the jets formed in passing through the screen openings. This deflection of the flow leads to an additional loss. As velocity increases (Reynolds number increases), the rods become more and more effective in deflecting the flow. This is illustrated by the curve representing screen No. 1 in Fig. 13 ($\beta = 75^{\circ}$) and further emphasized by the curves representing screens No. 1 and 3 in Fig. 14 ($\beta = 60^{\circ}$). As β increases to 60°, data points for screens 3 and 5 no longer fall on the same curve

In Fig. 13, for $\beta = 75^{\circ}$, screen No. 4 generally has a higher headloss coefficient than screen No. 1, since screen No. 4 has a smaller area of screen opening. As β decreases to 60° (Fig. 14), the effect of rod length has already overridden the contraction effect around the wires. The impact

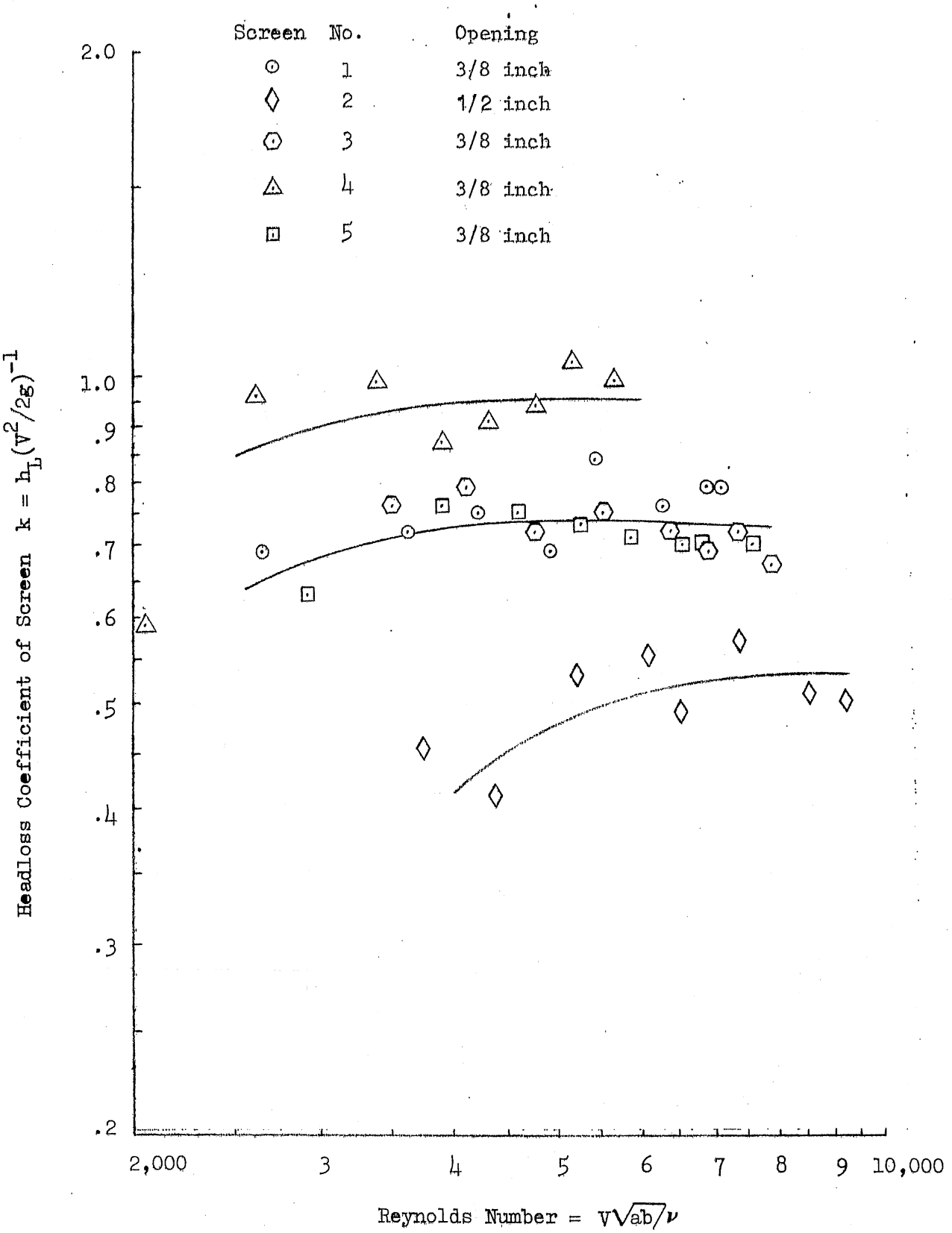

Fig. 9(a) - Headloss Coefficient of Screen Panels at Angle of Approach $\alpha = 90^{\circ}$.

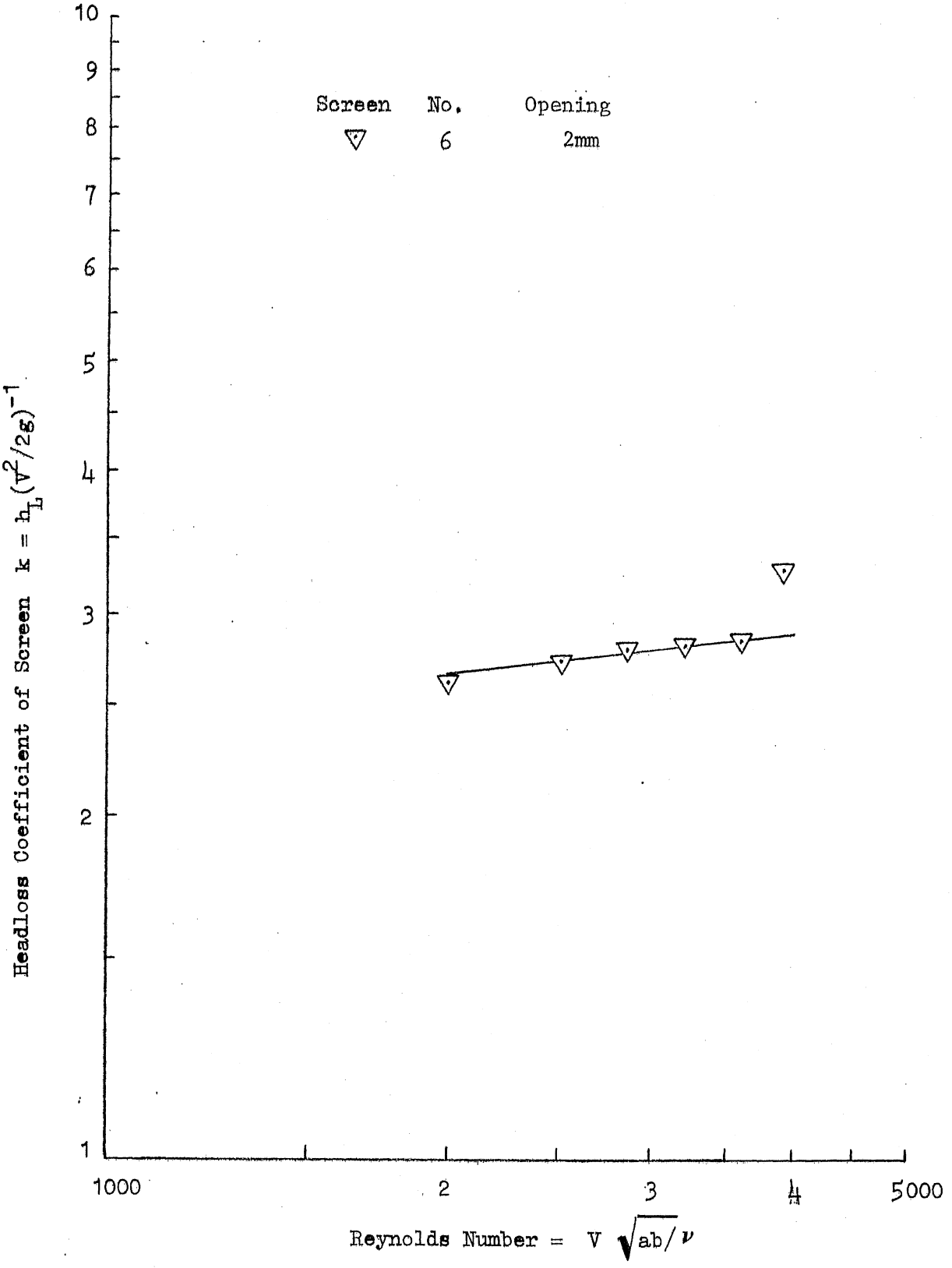

Fig. 9(b) - Headloss Coefficient of Screen Panel at Angle of Approach $\alpha = 90^{\circ}$.

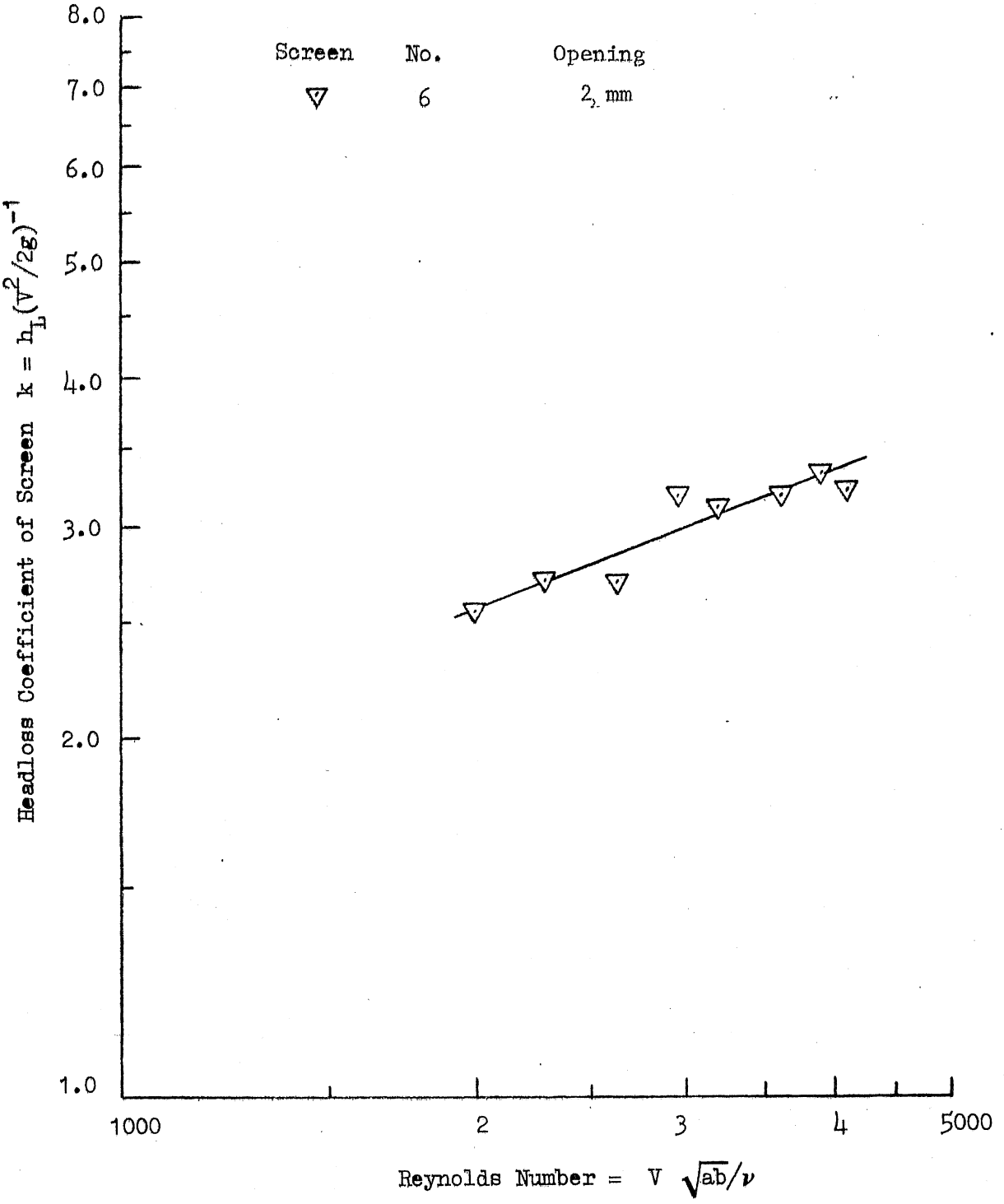

Fig. 10 - Headloss Coefficient of Screen Panel at Angle of Approach $\alpha = 75^{\circ}$.

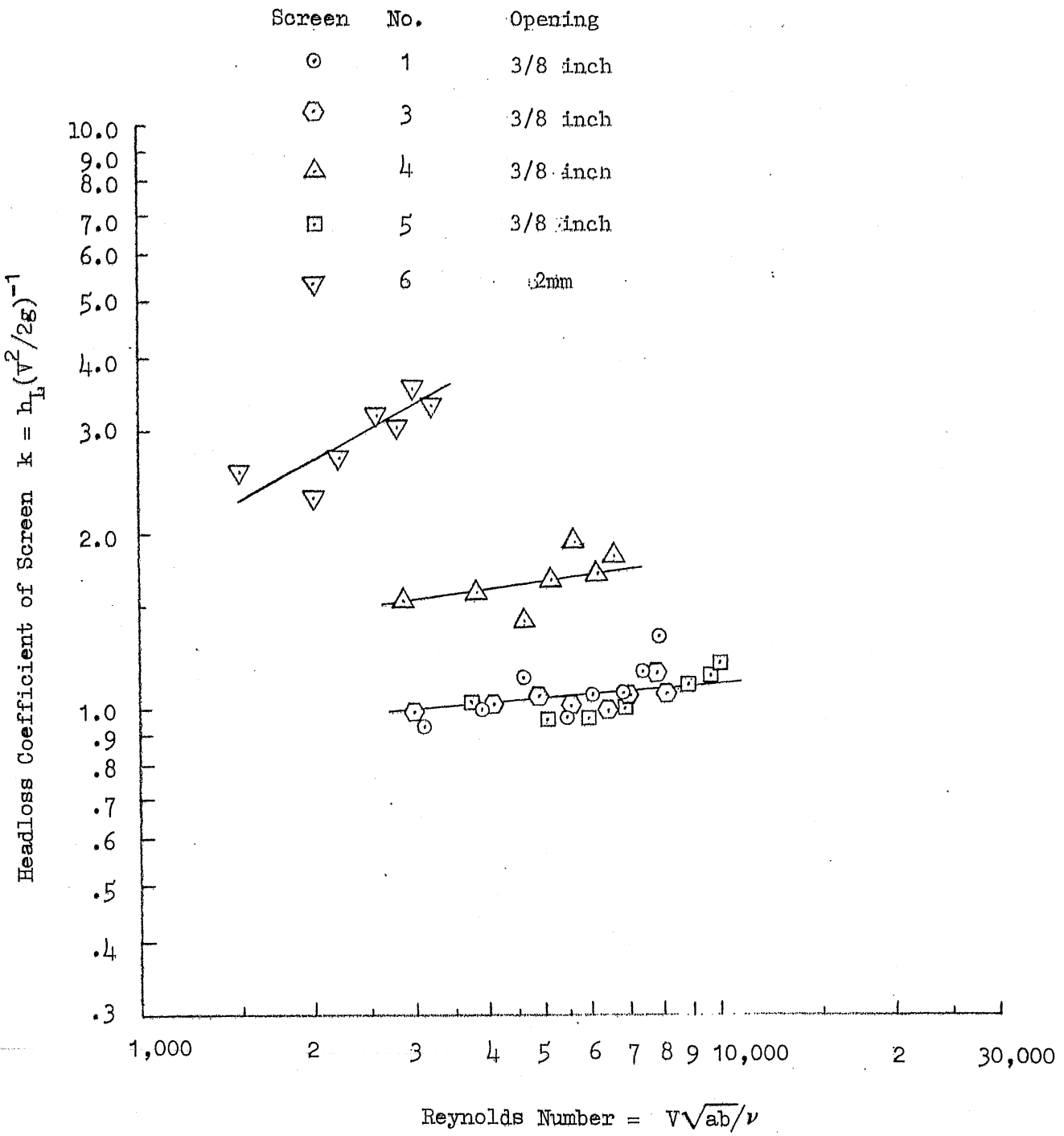

Fig. 11 - Headloss Coefficient of Screen Panels at Angle of Approach $\alpha = 60^{\circ}$.

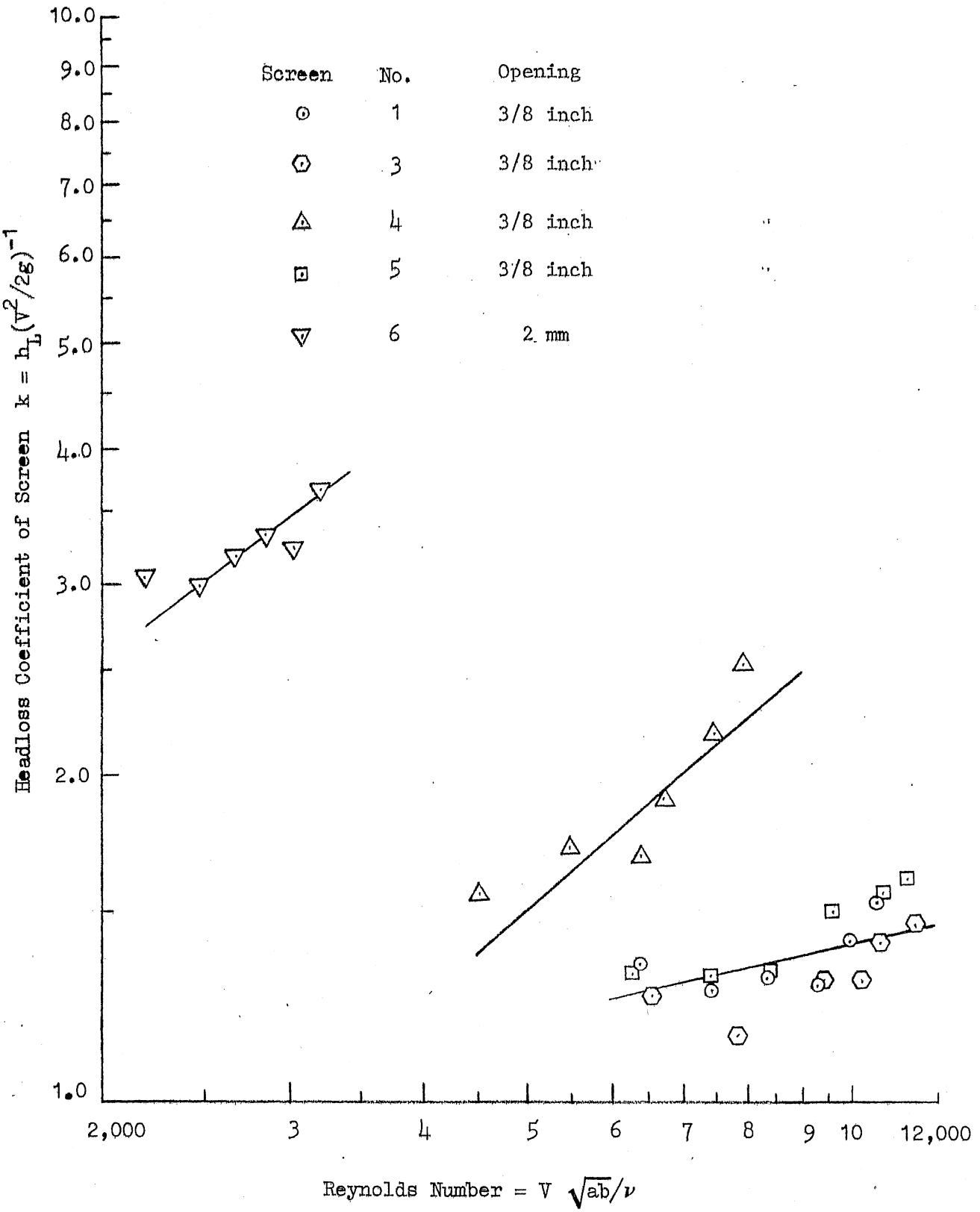

Fig. 12 - Headloss Coefficient of Screen Panels at Angle of Approach $\alpha = 45^{\circ}$.

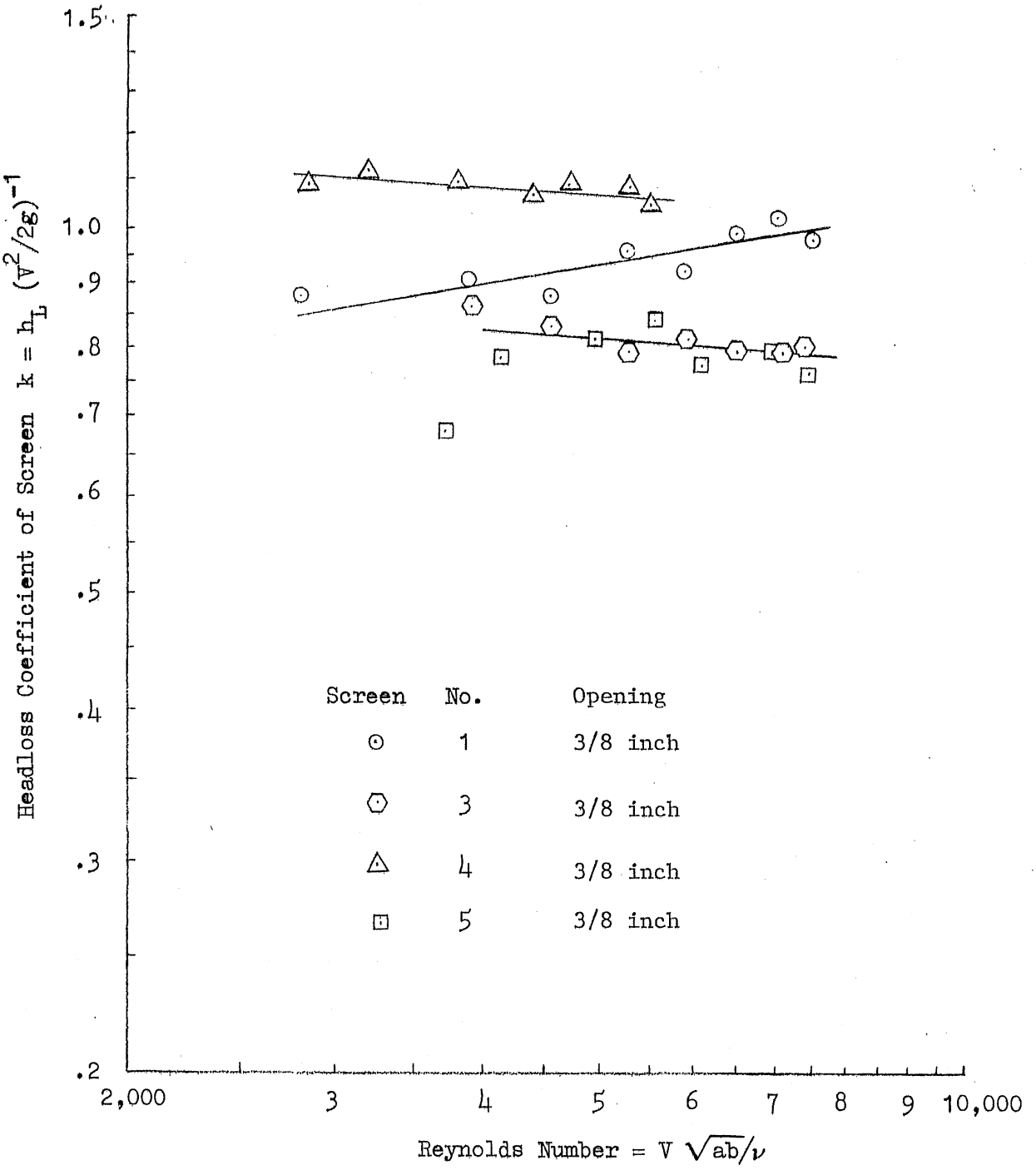

Fig. 13 - Headloss Coefficient of Screen Panels at Angle of Approach $\beta = 75^{\circ}$.

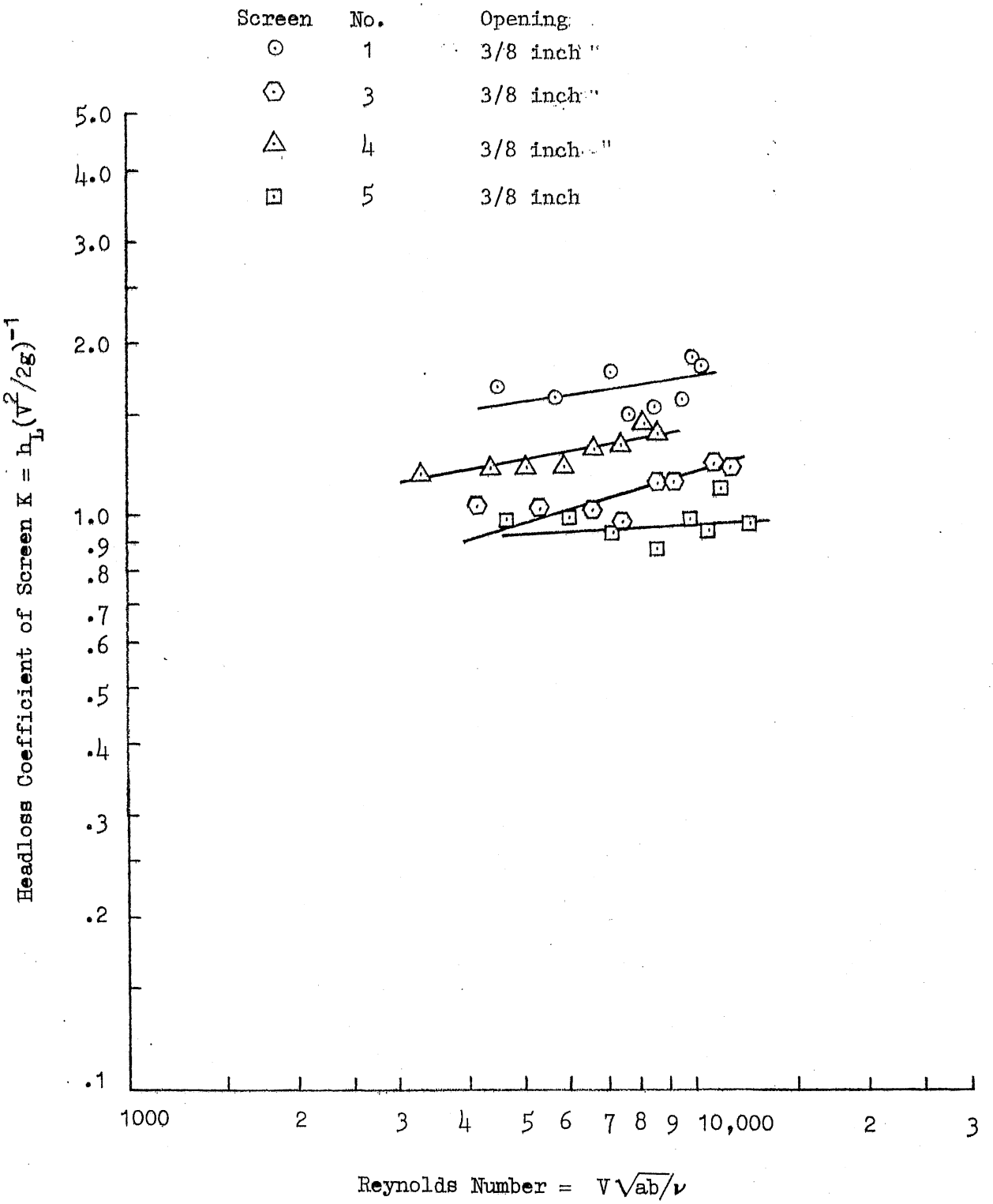

Fig. 14 - Headloss Coefficient of Screen Panels at Angle of Approach $\beta = 60^{\circ}$.

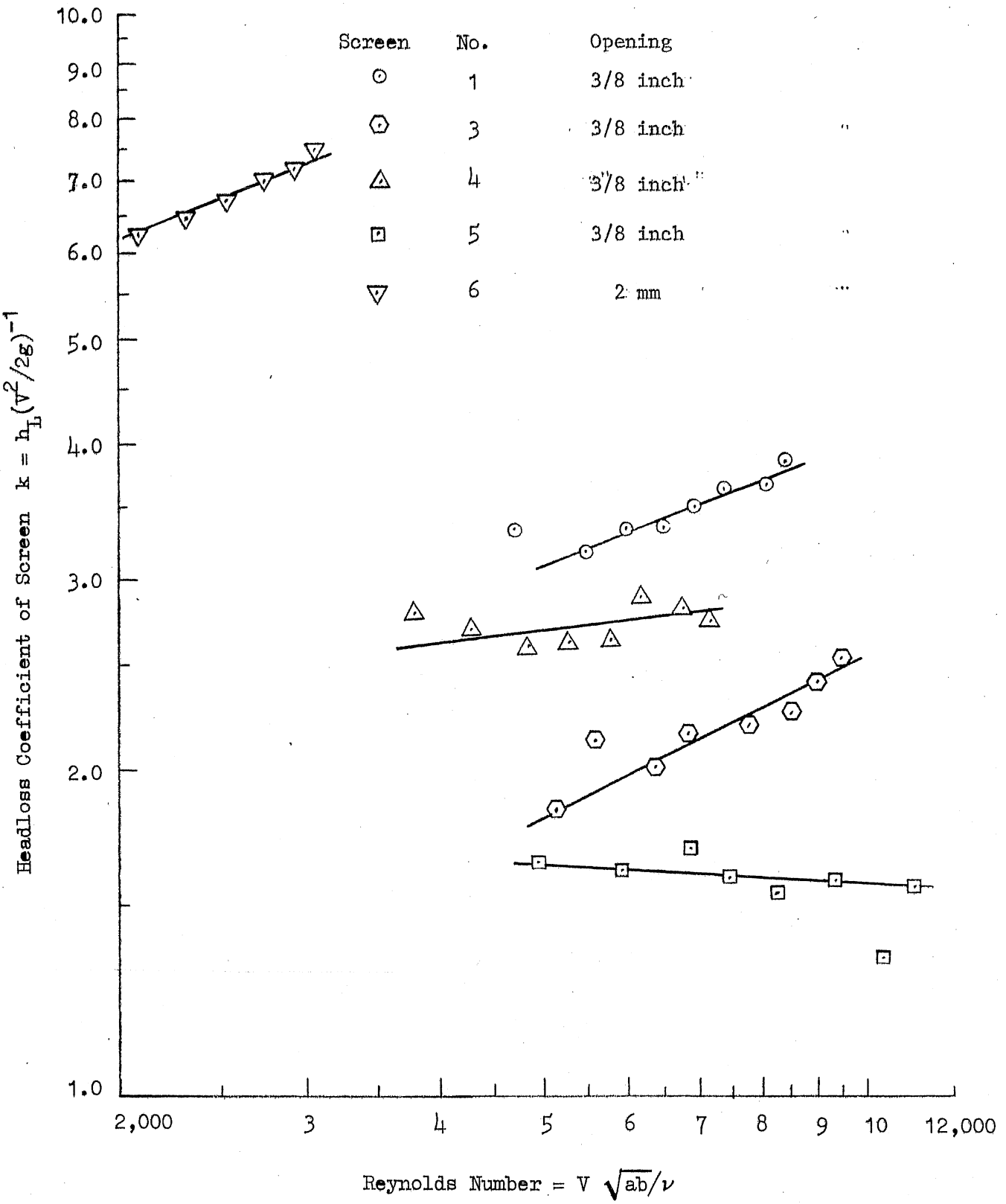

Fig. 15 - Headloss Coefficient of Screen Panels at Angle of Approach $\beta = 45^{\circ}$.

of the flow on the sidewalls of the experimental flume becomes significant and a limitation to the accuracy of the data. At $\beta = 60^{\circ}$, screen No. 1 has the largest headloss coefficient among screens No. 1, 3, 4, and 5, and the headloss coefficient for screen No. 3 (rod length = 0.5") now comes closer to that of screen No. 4 (rod length = 0.2") as compared to the difference at $\beta = 75^{\circ}$ (Fig. 13).

At $\beta = 75^{\circ}$, all the screens have headloss coefficients slightly higher than those at $\alpha = 90^{\circ}$. At $\beta = 60^{\circ}$, the differences are even larger.

Design curves for all screen panels have been prepared. These curves are in the form of headloss as a function of reference approach velocity and are shown in Figs. 16 through 22. Curves at 32°F water temperature represent winter conditions, while curves at 75°F water temperature represent approximate summer conditions. In the velocity range from 0.5 to 2.5 ft/sec summer losses are generally shown slightly higher than winter losses because lower water viscosity in summer gives higher Reynolds numbers which in turn gives higher loss coefficients in Figs. 9 through 14. Graphs are provided for different angles of approach α and β. The reference approach velocity is defined as the flow rate divided by screen panel area. Its value is independent of the orientation of the screen.

VIII. Fundamental and Theoretical Considerations for Flow Through Screens

The literature referred to in an earlier section and other studies not specifically referred to herein contain theoretical attempts to predict headloss coefficients by application of fundamental hydrodynamic principles. Prerequisites for such efforts include some knowledge of the qualitative features and kinetics of flow through a screen, and the acceptance of simplifications and hypothesis regarding the geometry and the flow field. Theoretical analysis may not be carried through without introduction of some experimental coefficients for many types of screens. Despite this obvious deficiency, it would appear of value to a designer or manufacturer at one time or another to engage in some more fundamental analysis of a screen design.

(1) Mechanism of Screen Flow

The flow is accelerated when it passes through the screen due to the constriction imposed by the screen, and forms jets of higher than approach velocity behind the openings, interspersed with wakes of relatively

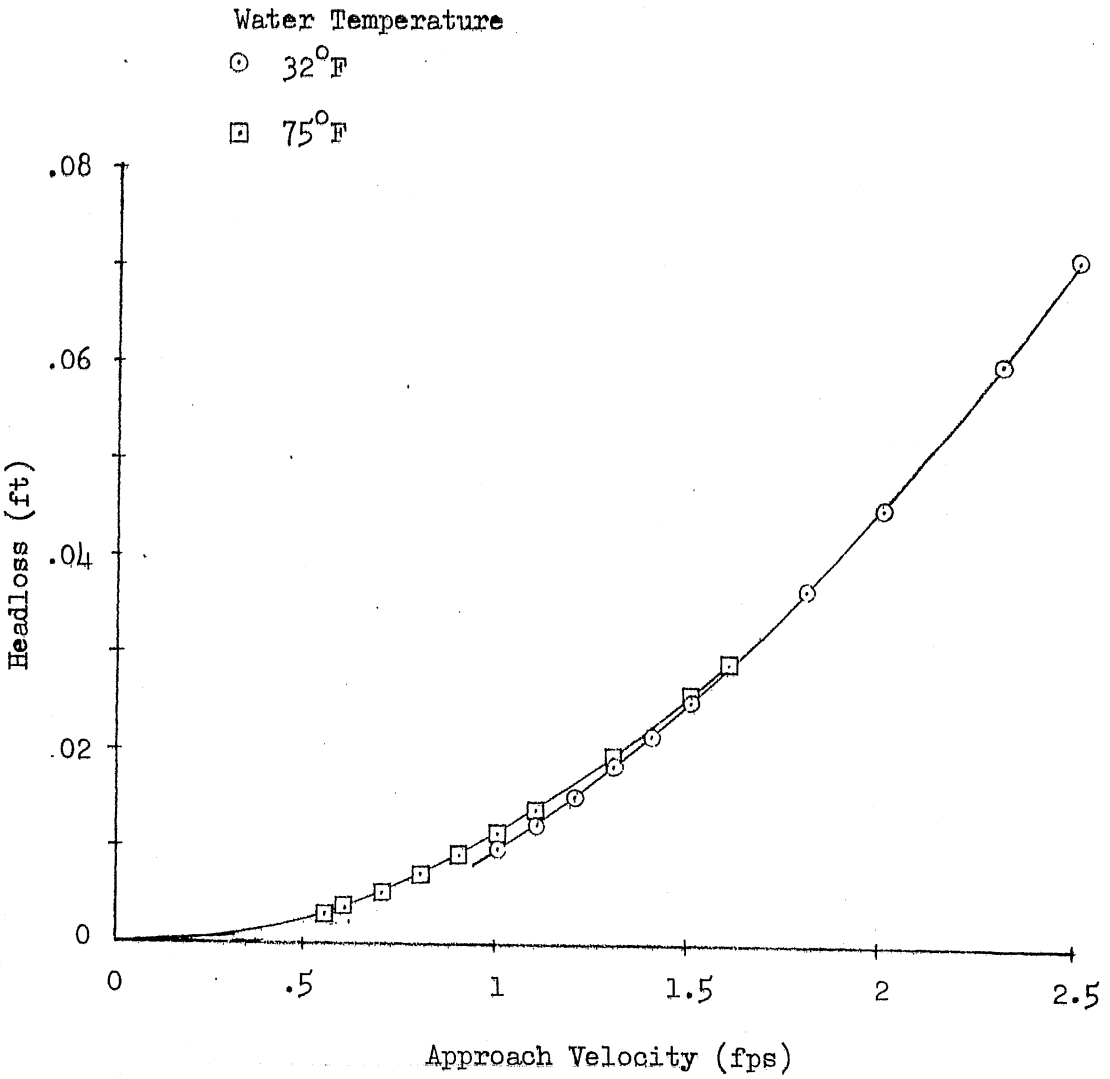

Fig. 16(a) - Headloss of Screen Panels Nos. 1, 3, and 5 (15/16" x 3/8" opening) at Angle of Approach $\alpha = 90^{0}$.

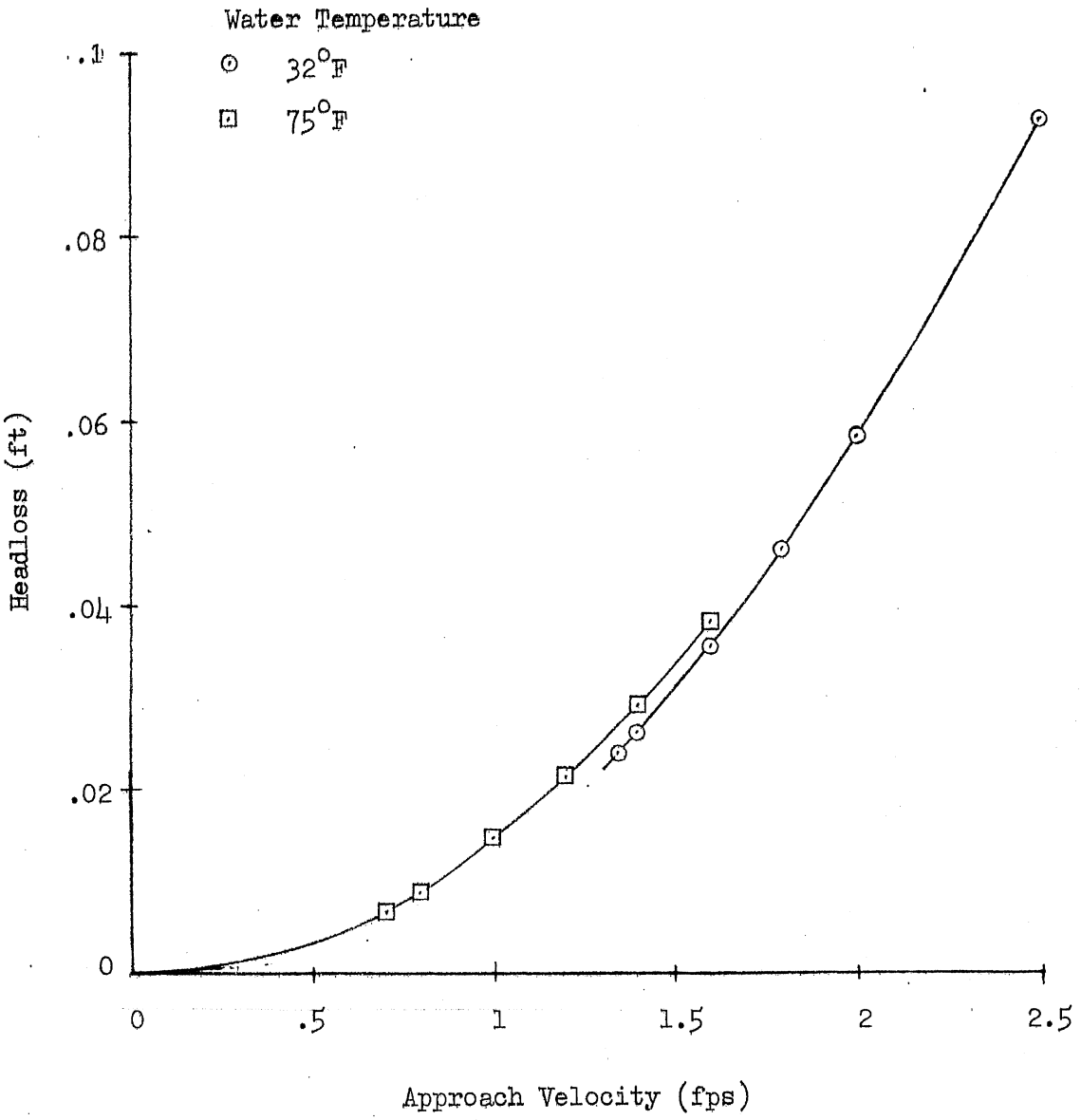

Fig. 16(b) Headloss of Screen Panel No. 4 (3/8" x 3/8" opening) at Angle of Approach $\alpha = 90^{\circ}$.

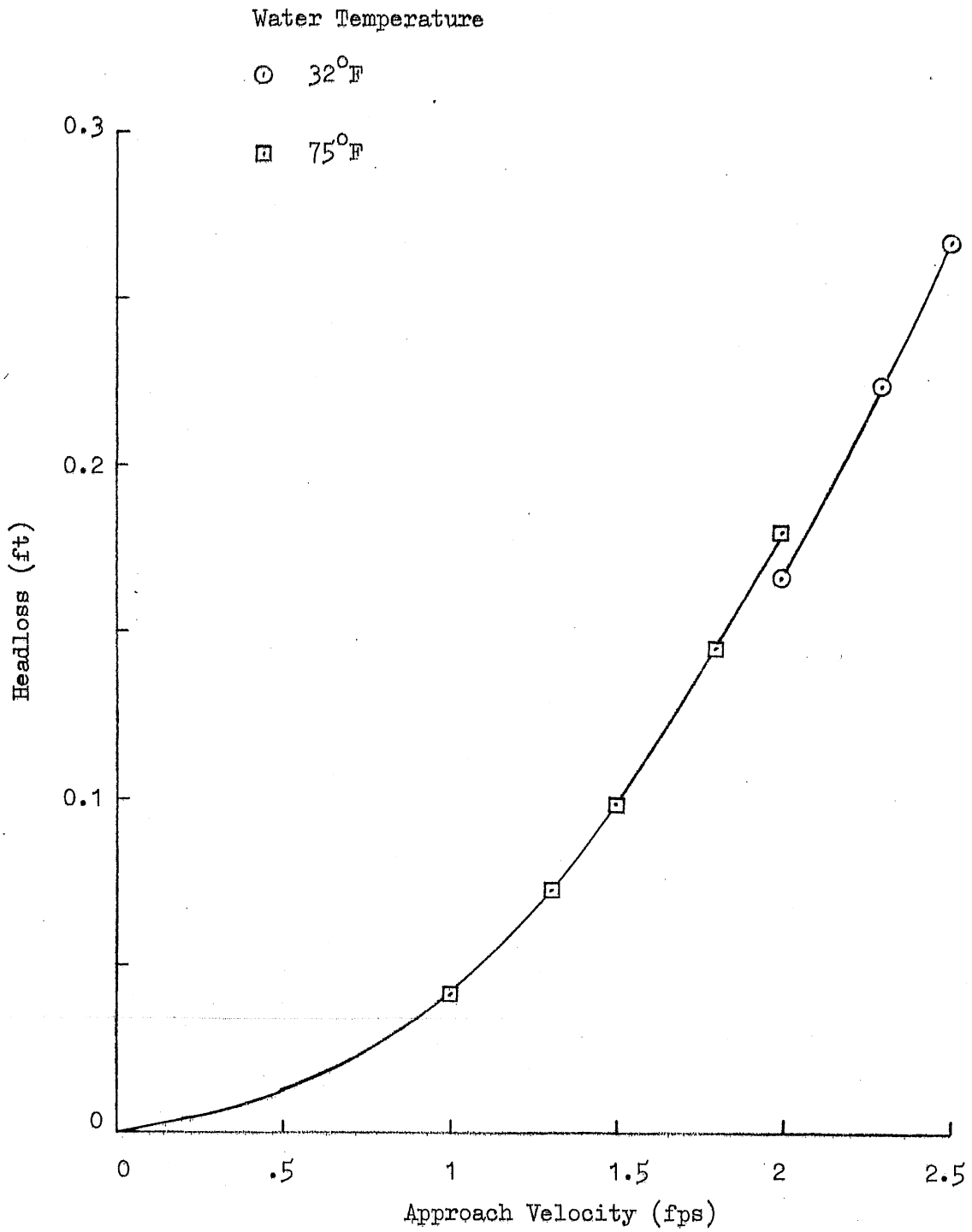

Fig. 16(c) - Headloss of Screen Panel No. 6 (2 mm opening) at Angle of Approach $\alpha = 90^{\circ}$.

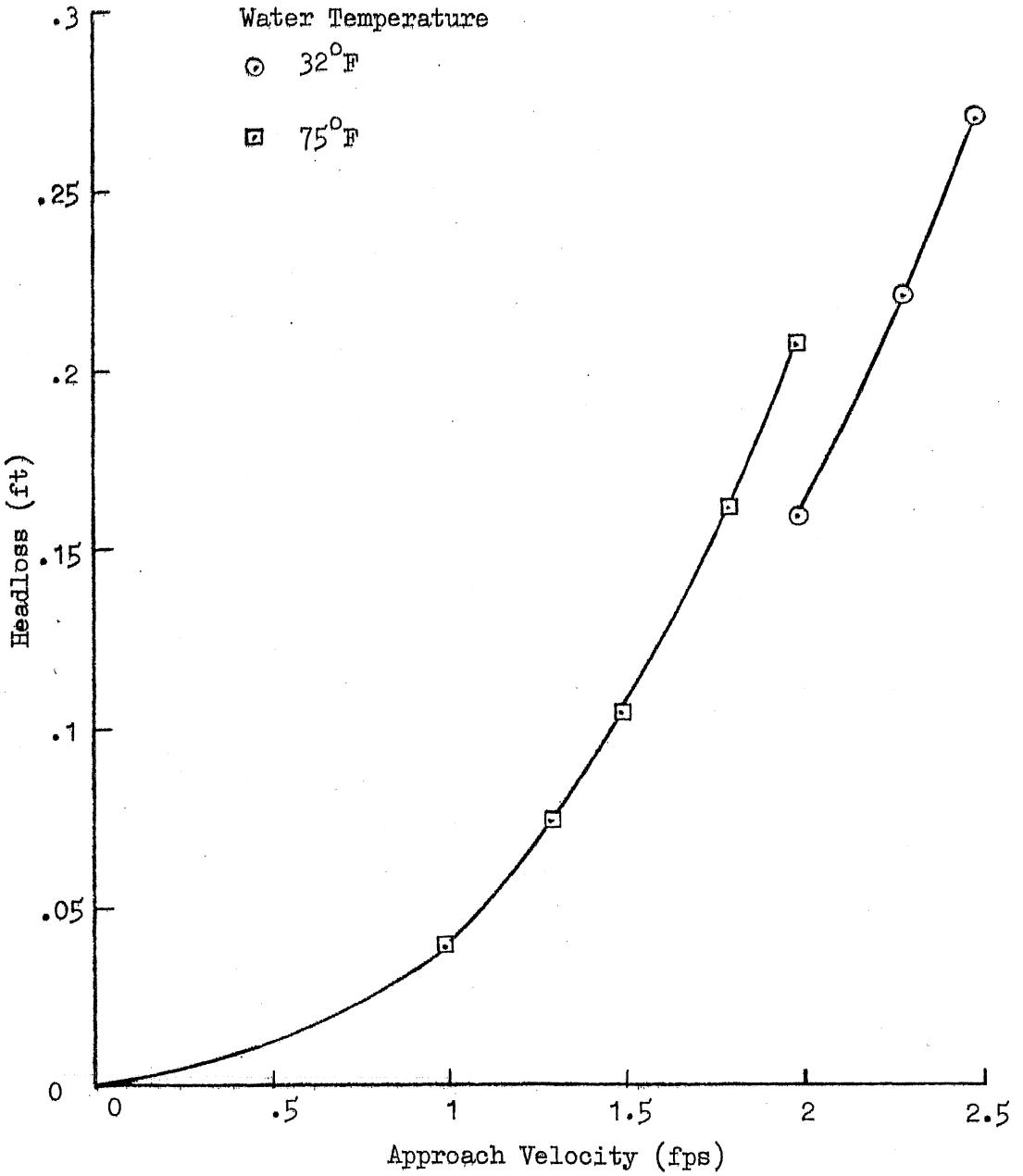

Fig. 17 - Headloss of Screen Panel No. 6 (2mm opening) at Angle of Approach $\alpha = 75^{\circ}$.

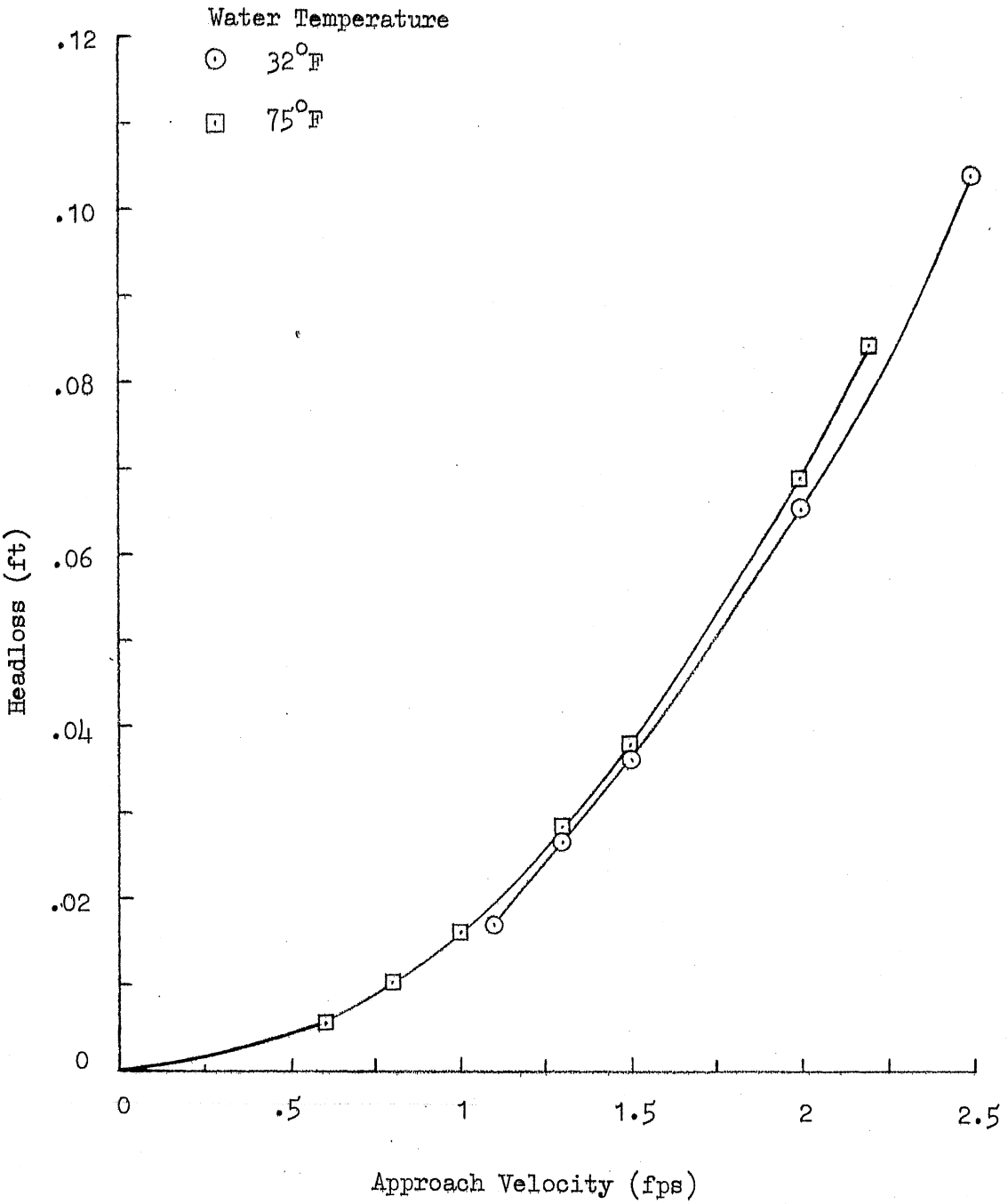

Fig. 18(a) - Headloss of Screen Panels Nos. 1, 3, and 5 (7/8" x 3/8" opening) at Angle of Approach $\alpha = 60^{\circ}$.

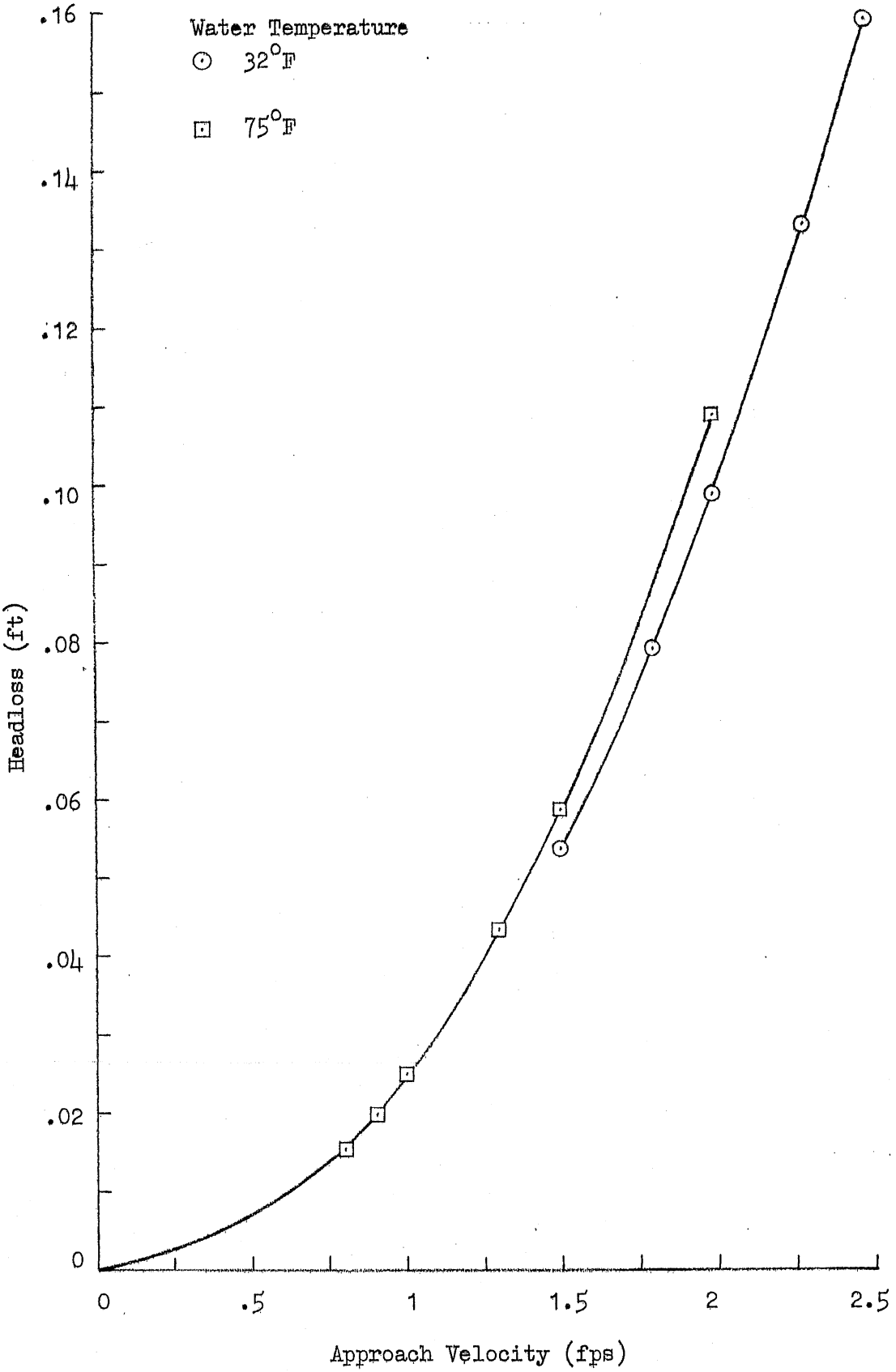

Fig. 18(b) - Headloss of Screen Panel No. 4 (3/8" x 3/8" opening) at Angle of Approach $\alpha = 60^{\circ}$.

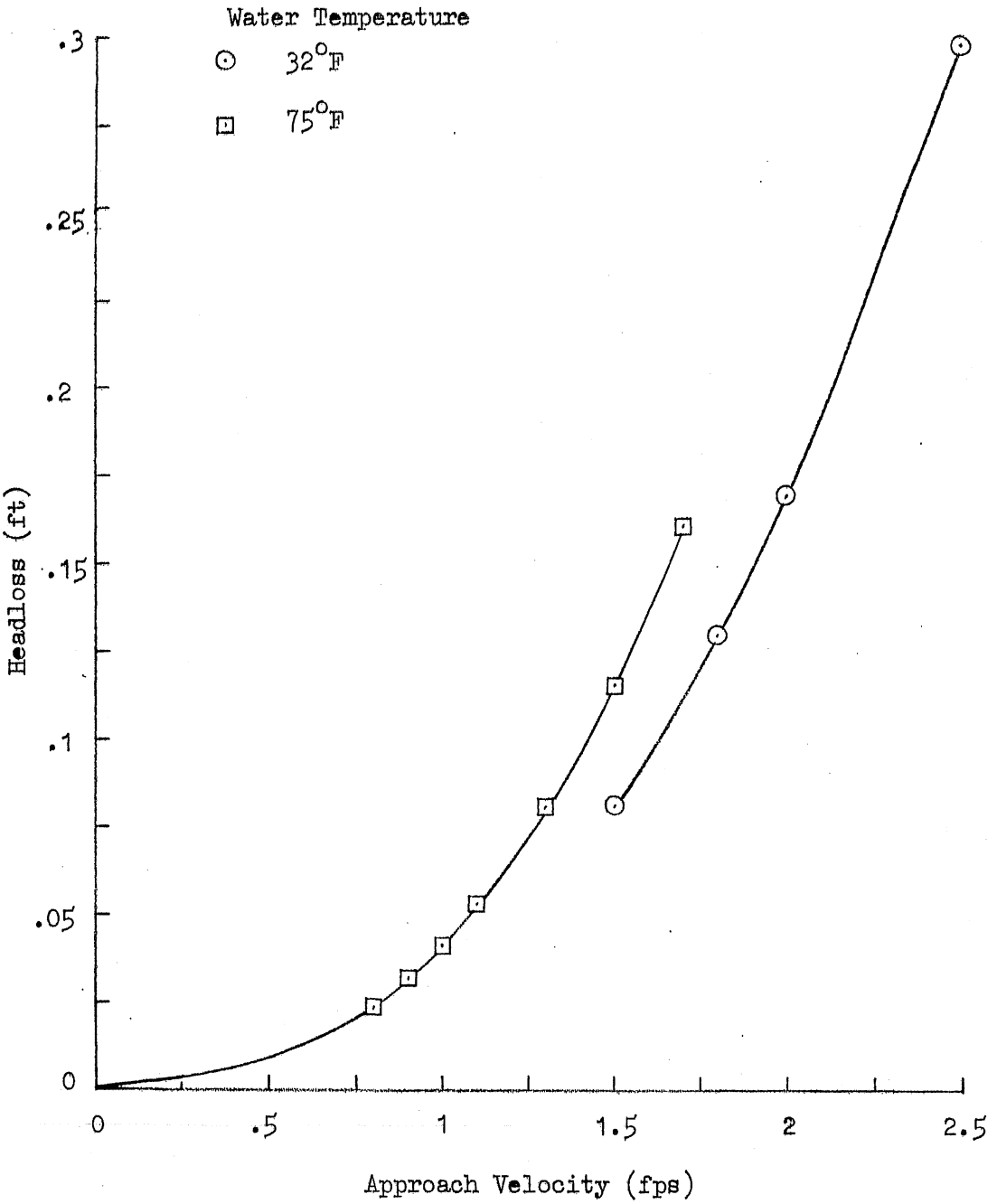

Fig. 18(c) - Headloss of Screen Panel No. 6 (2mm opening) at Angle of Approach $\alpha = 60^{\circ}$.

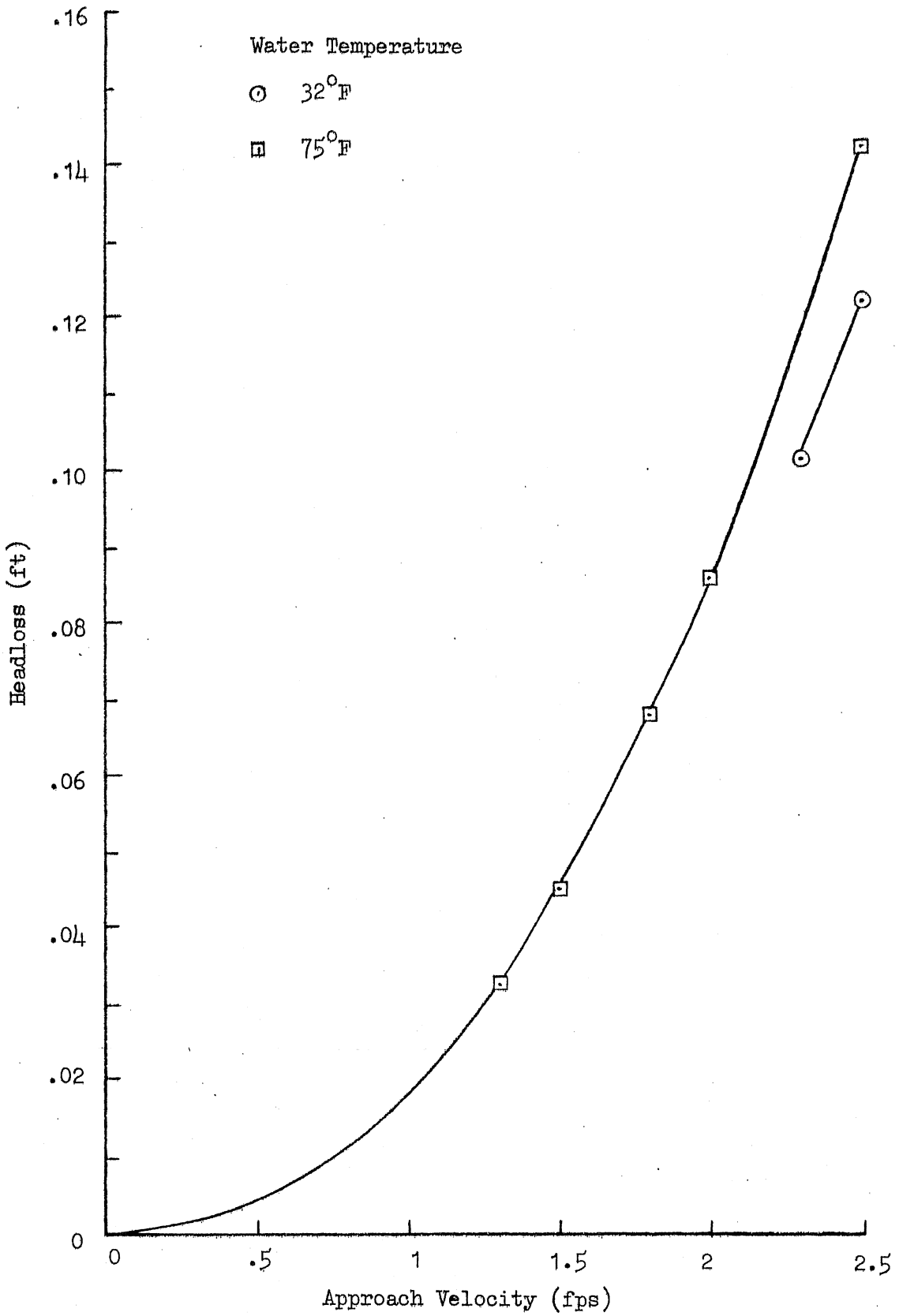

Fig. 19(a) - Headloss of Screen Panels Nos. 1, 3, and 5 (7/8" x 3/8" opening) at Angle of Approach $\alpha = 45^{o}$.

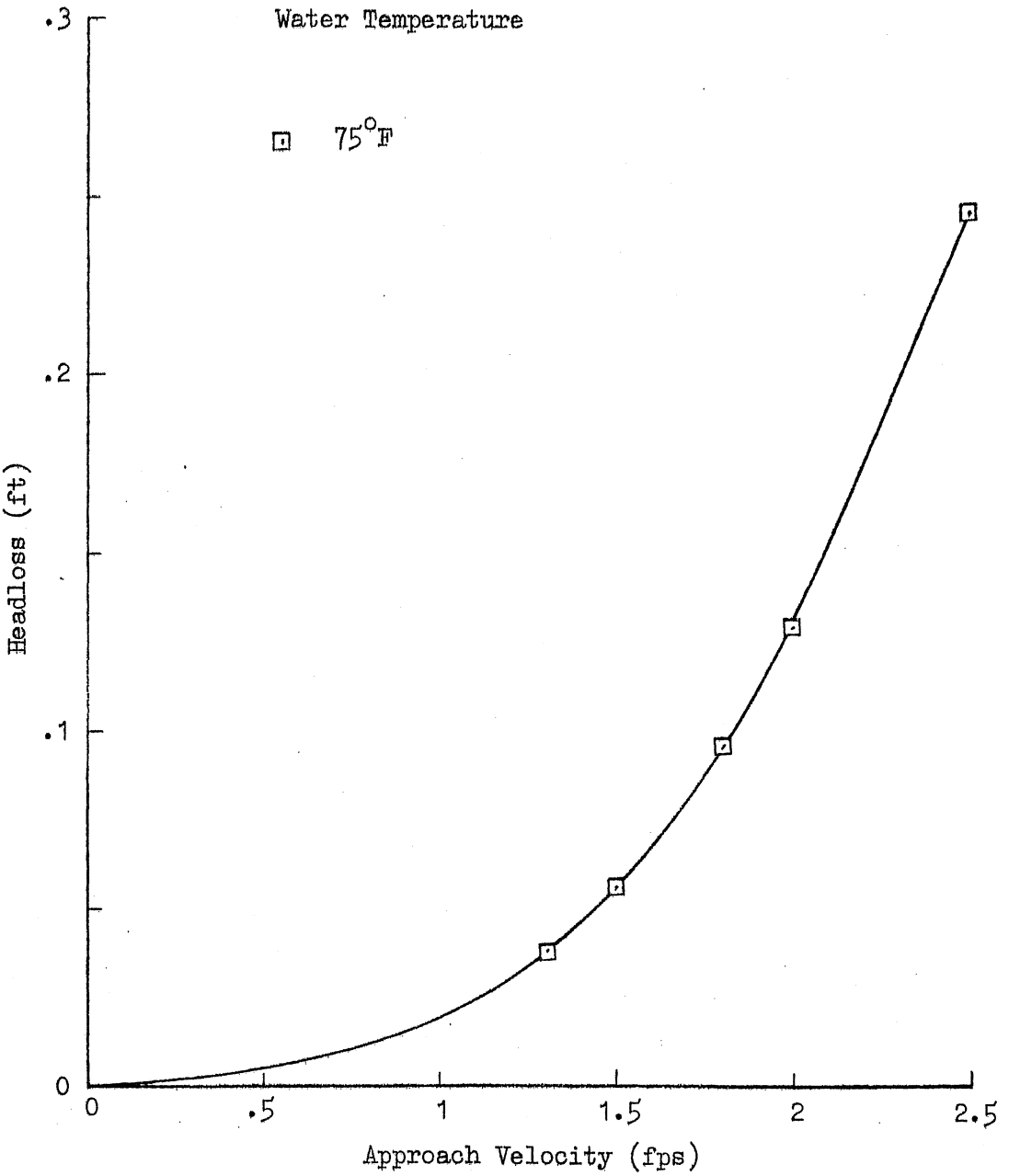

Fig. 19(b) - Headloss of Screen Panel No. 4 (3/8" x 3/8" opening) at Angle of Approach $\alpha = 45^{\circ}$.

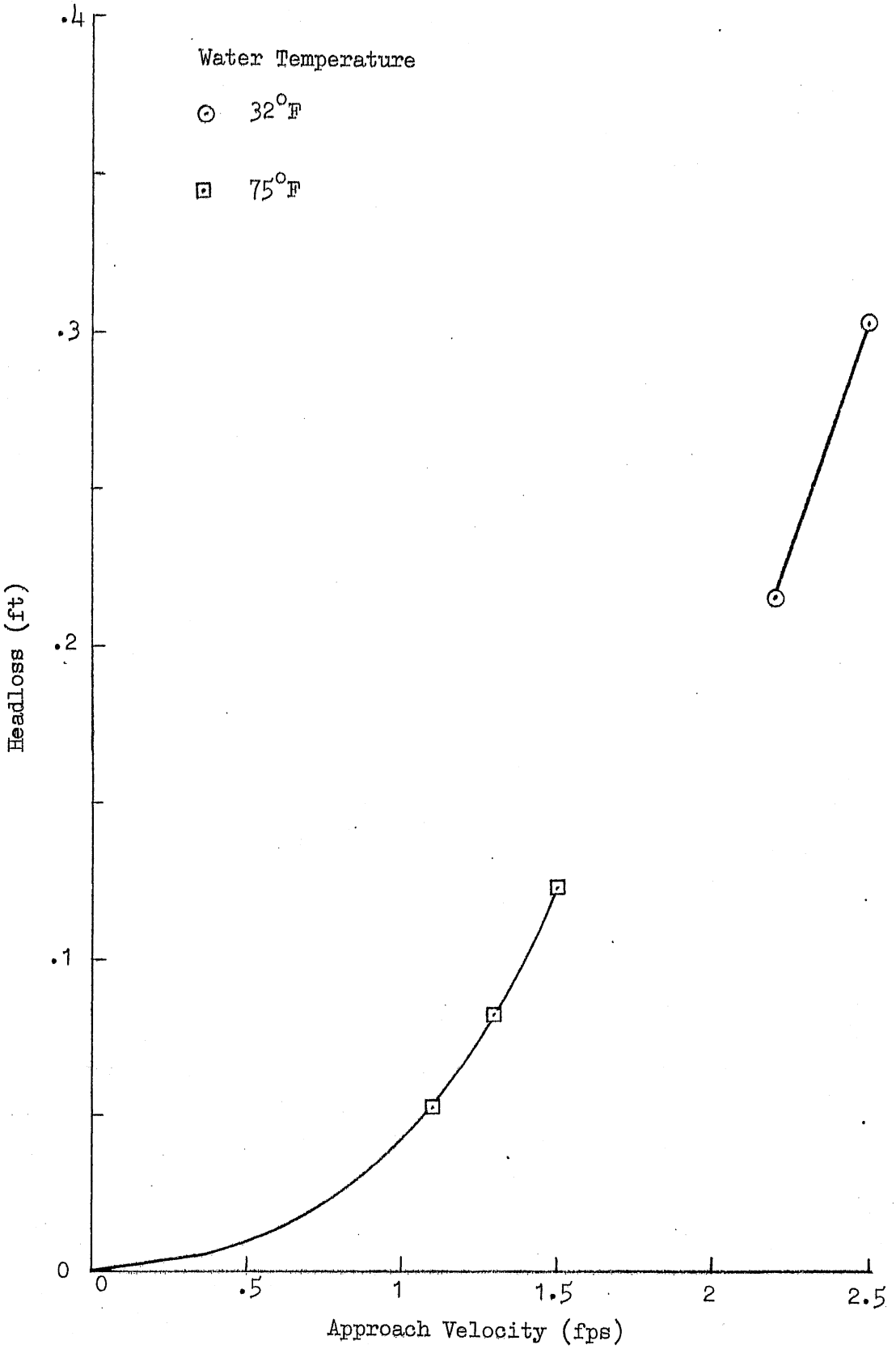

Fig. 19(c) - Headloss of Screen Panel No. 6 (2mm opening) at Angle of Approach $\alpha = 45^{\circ}$.

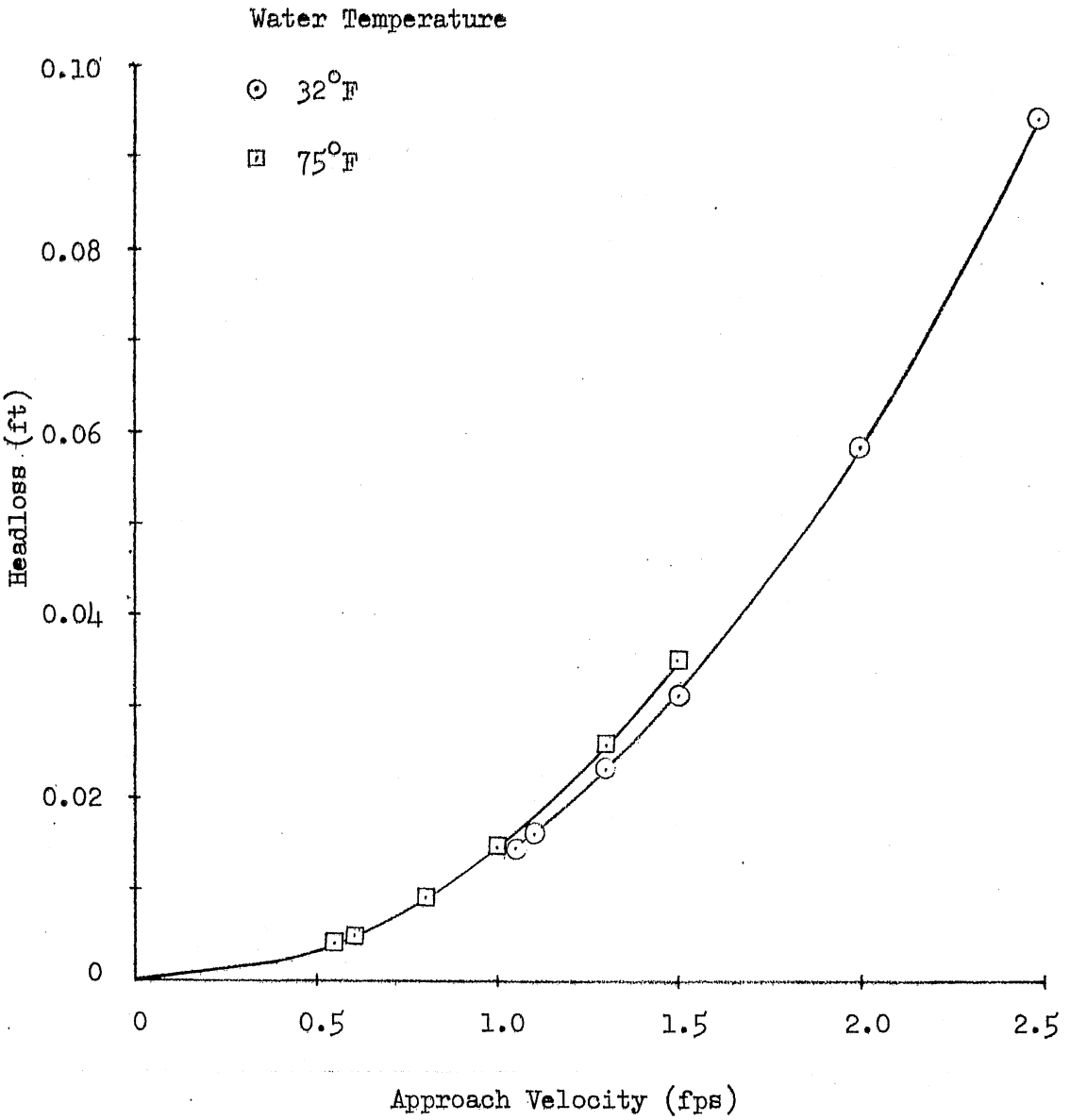

Fig. 20(a) - Headloss of Screen Panel No. 1 (15/16" x 3/8" opening) at Angle of Approach $\beta = 75^{\circ}$.

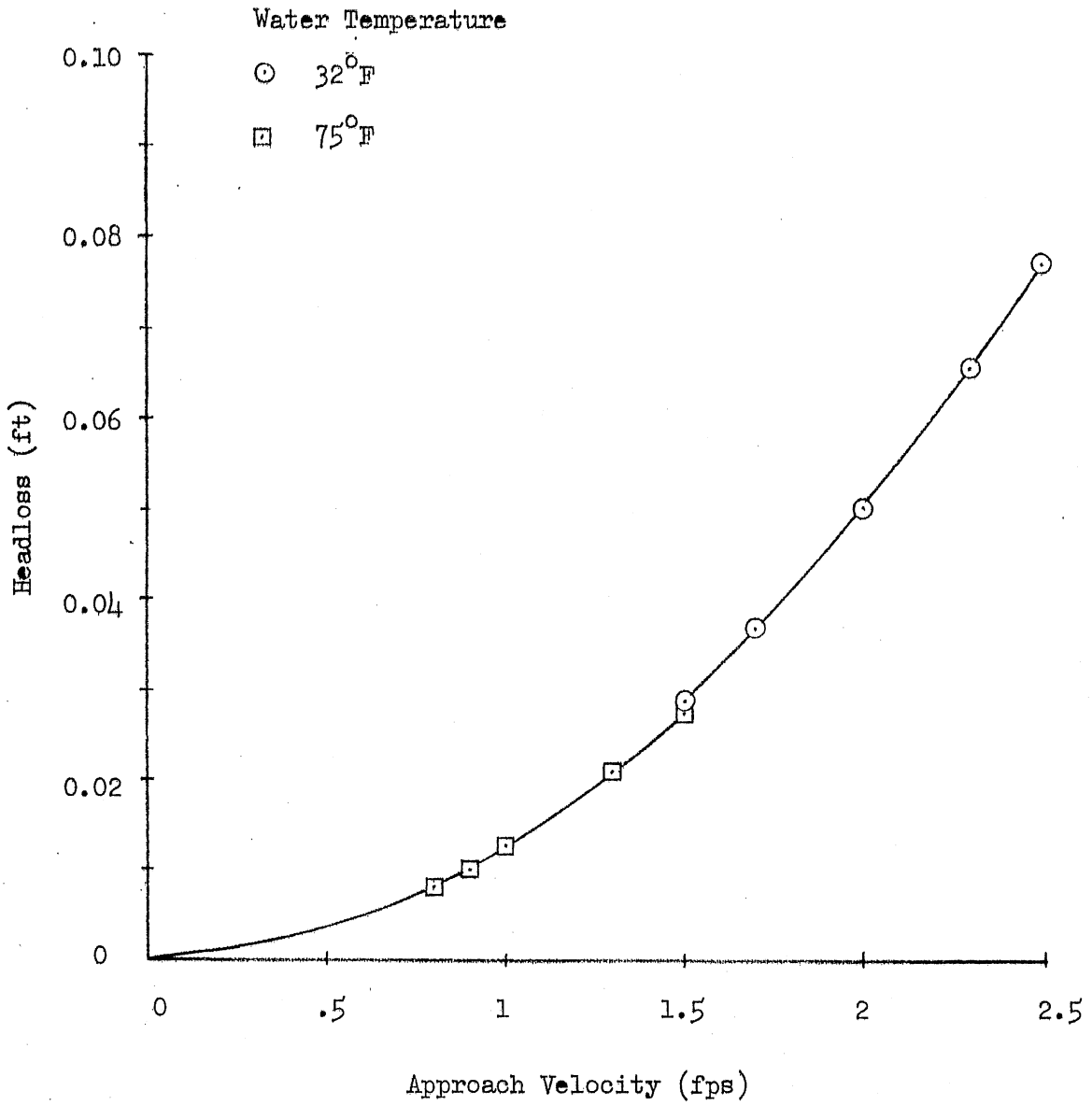

Fig. 20(b) - Headloss of Screen Panels No. 3 and 5 (7/8" x 3/8" opening) at Angle of Approach $\beta = 75^{\circ}$.

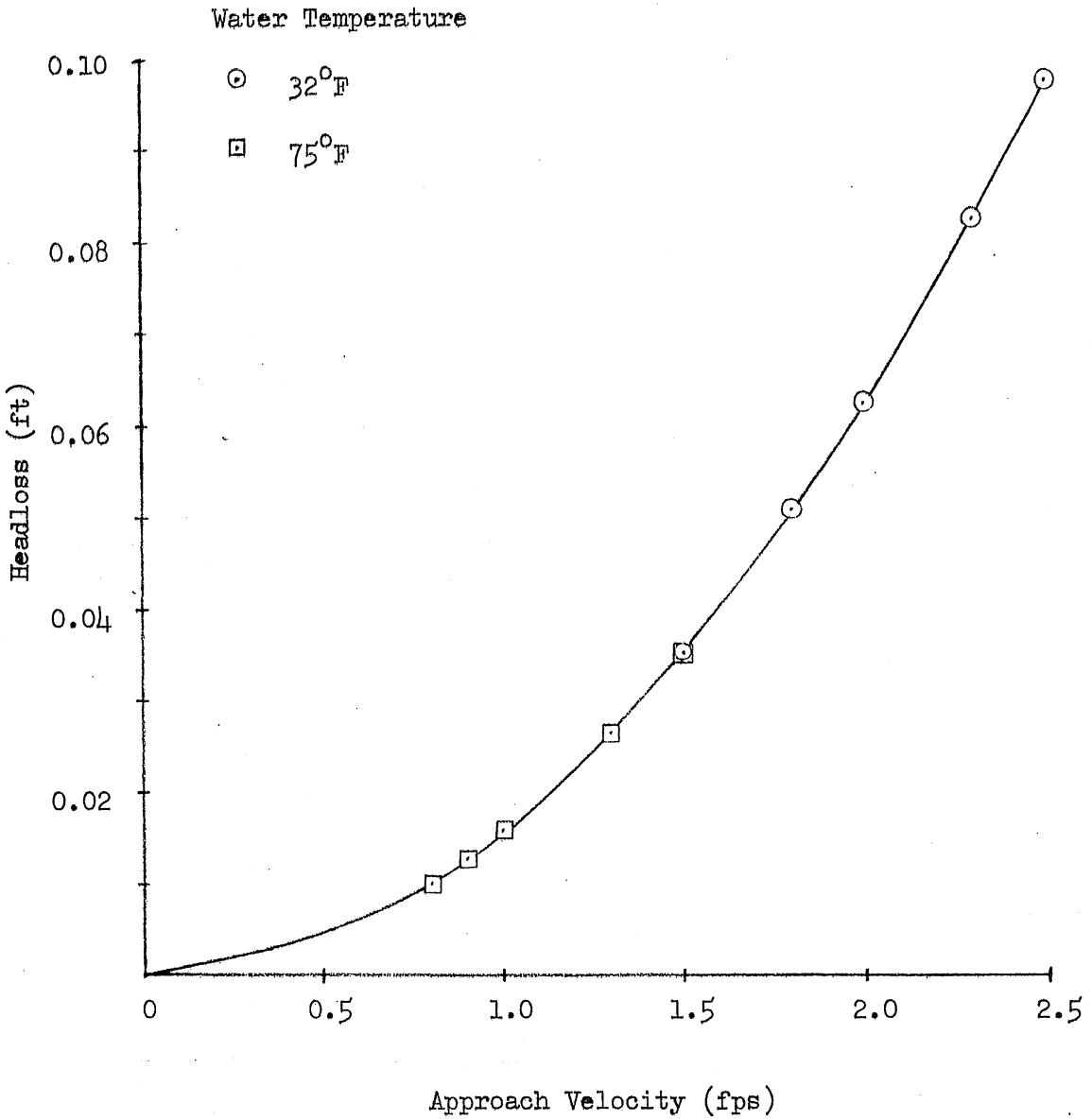

Fig. 20(c) - Headloss of Screen Panel No. 4 (3/8" x 3/8" opening at Angle of Approach $\beta = 75^{\circ}$.

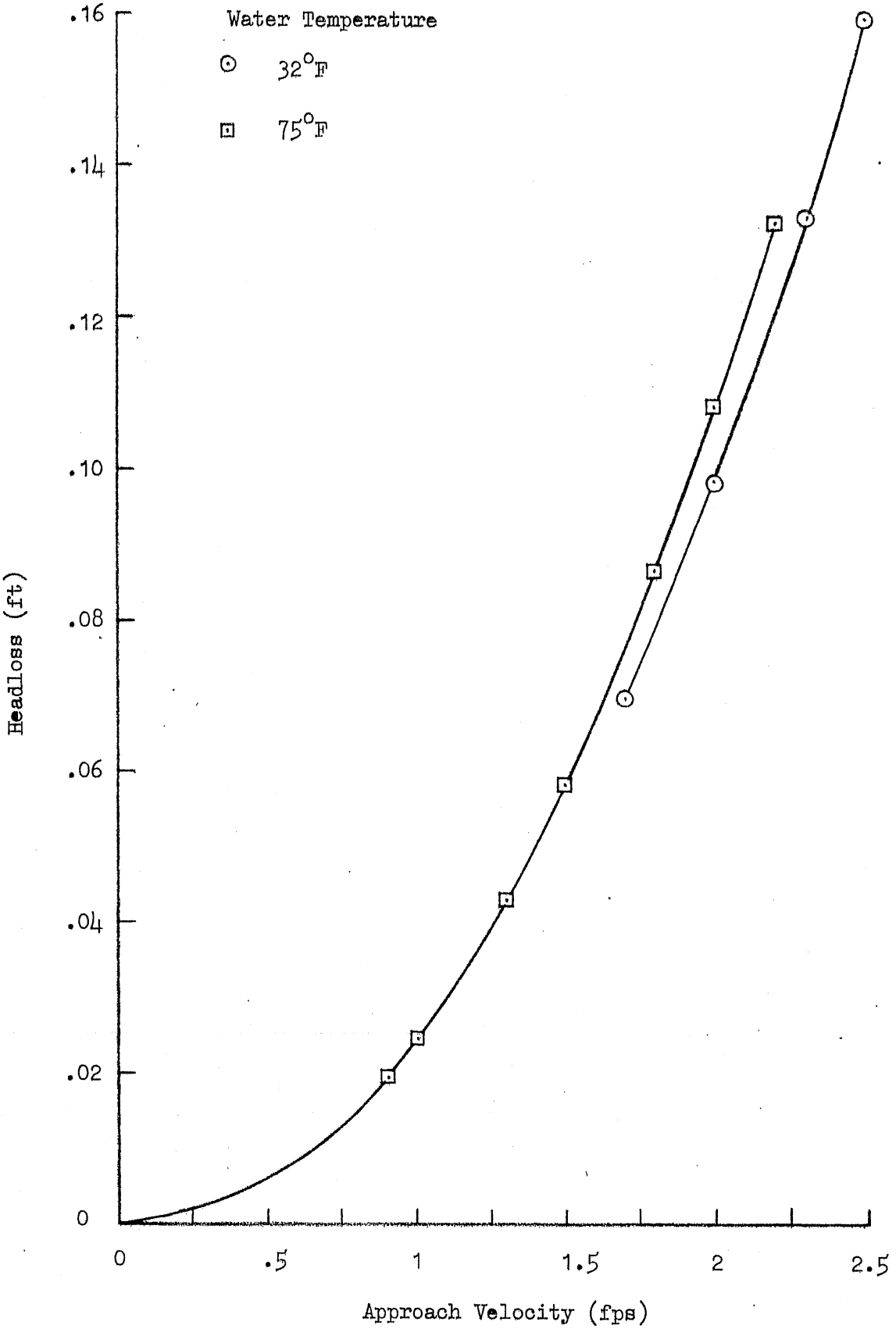

Fig. 21(a) - Headloss of Screen Panel No. 1 (15/16" x 3/8" opening) at Angle of Approach $\beta = 60^{\circ}$.

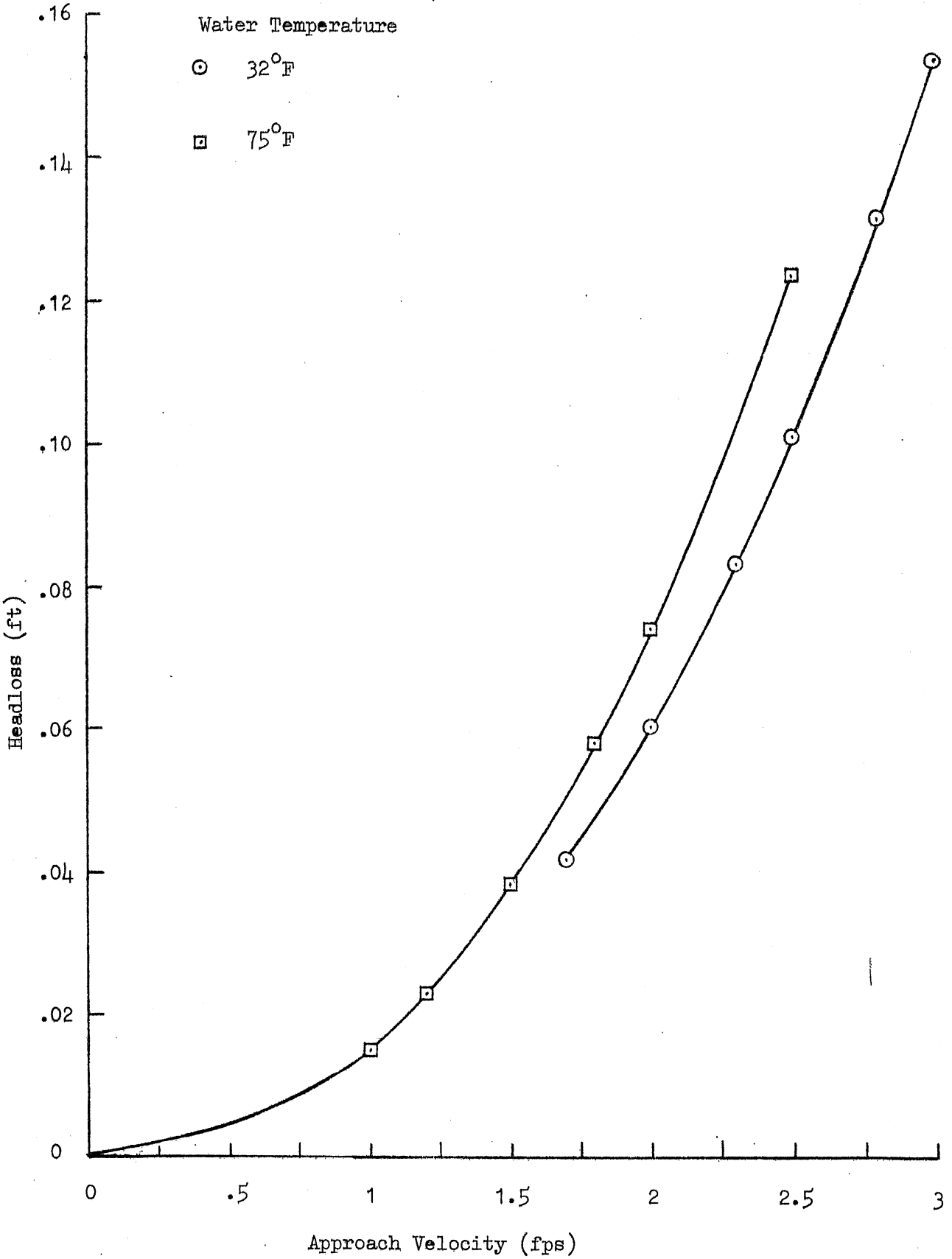

Fig. 21(b) - Headloss of Screen Panel No. 3 (15/16" x 3/8" opening) at Angle of Approach $\beta = 60^{\circ}$.

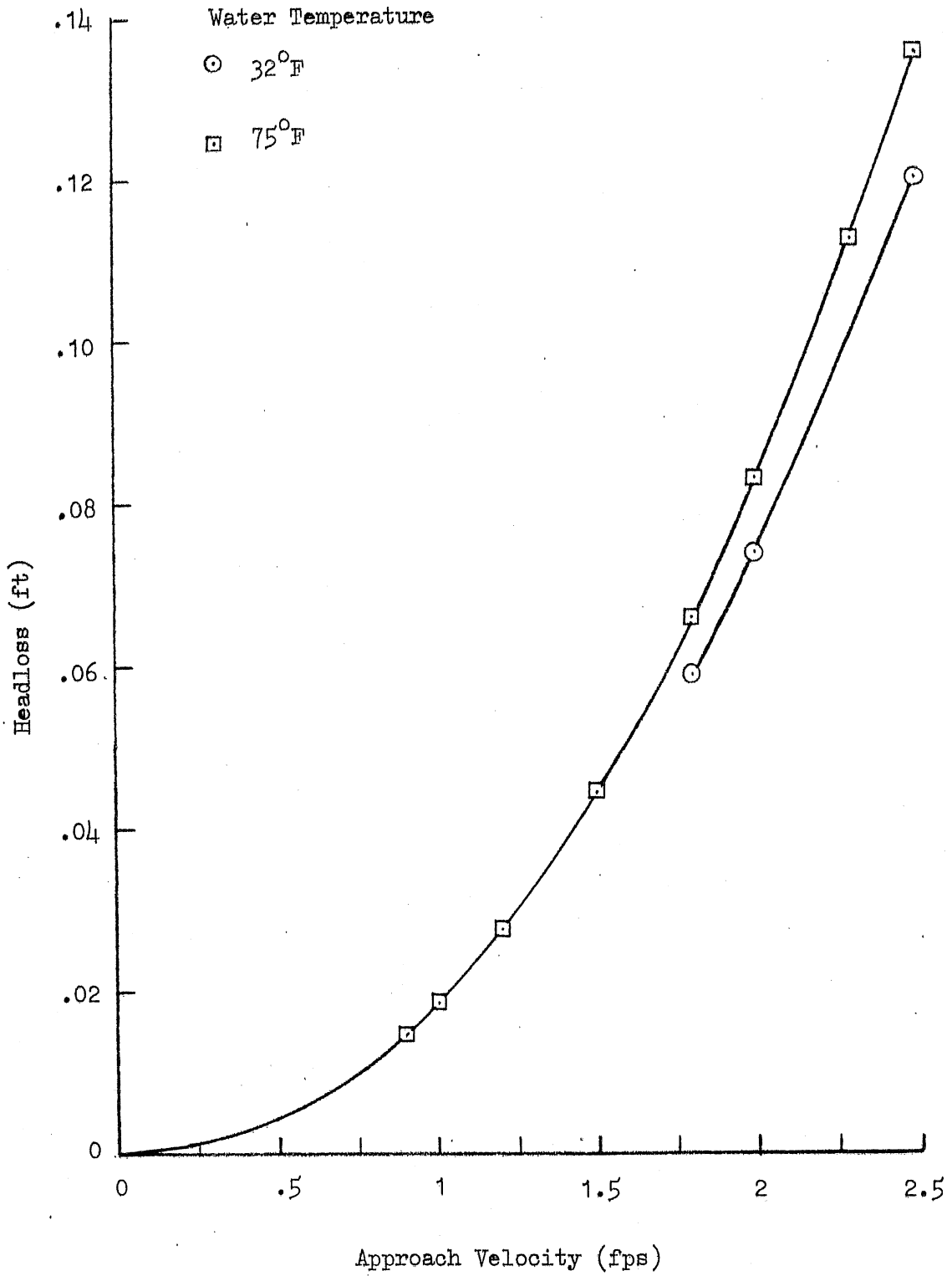

Fig. 21(c) - Headloss of Screen Panel No. 4 (3/8" x 3/8" opening) at Angle of Approach $\beta = 60^{\circ}$.

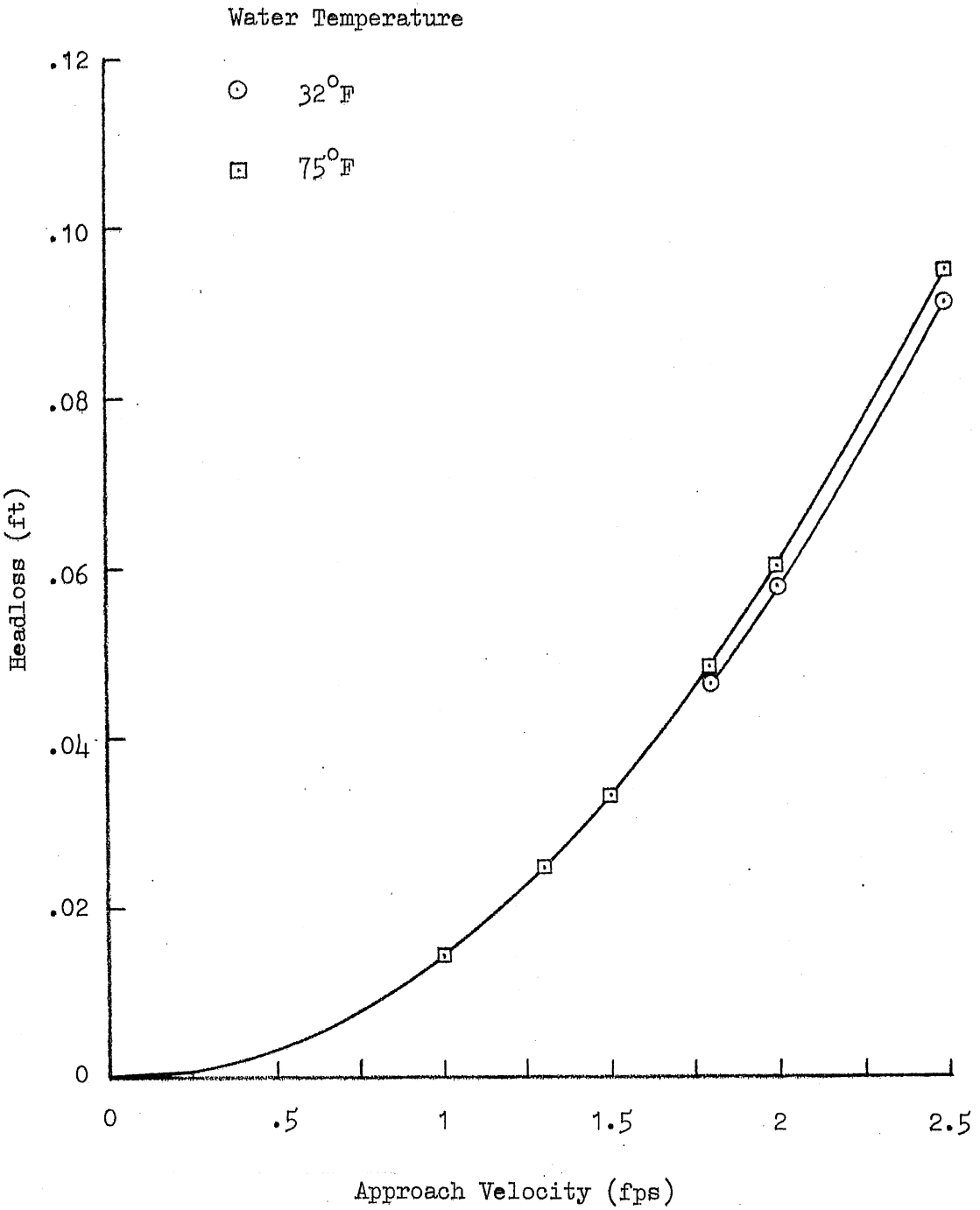

Fig. 21(d) - Headloss of Screen Panel No. 5 (7/8" x 3/8" opening) at Angle of Approach $\beta = 60^{\circ}$.

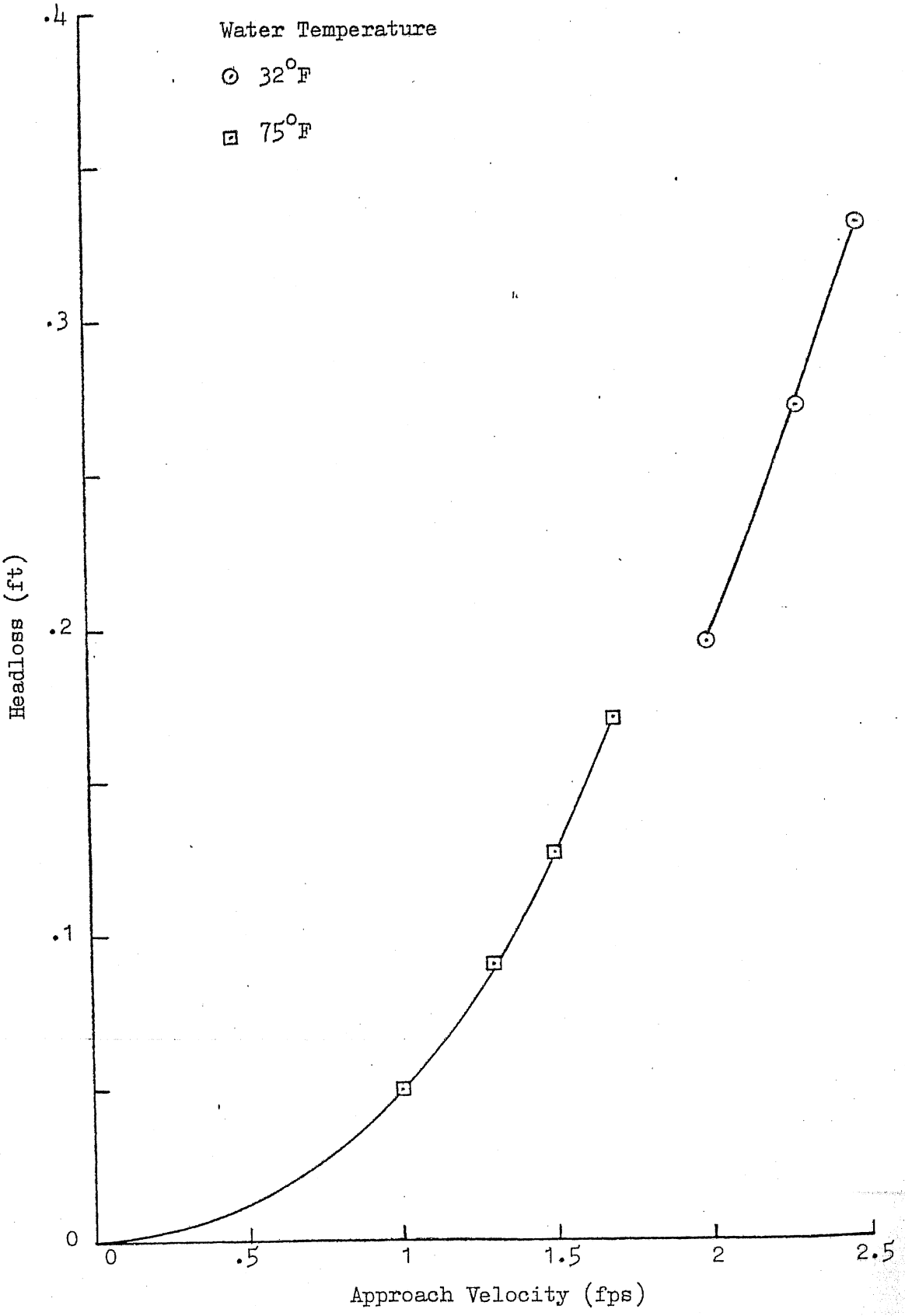

Fig. 22(a) - Headloss of Screen Panel No. 1 (15/16" x 3/8" opening) at Angle of Approach $\beta = 45^{o}$.

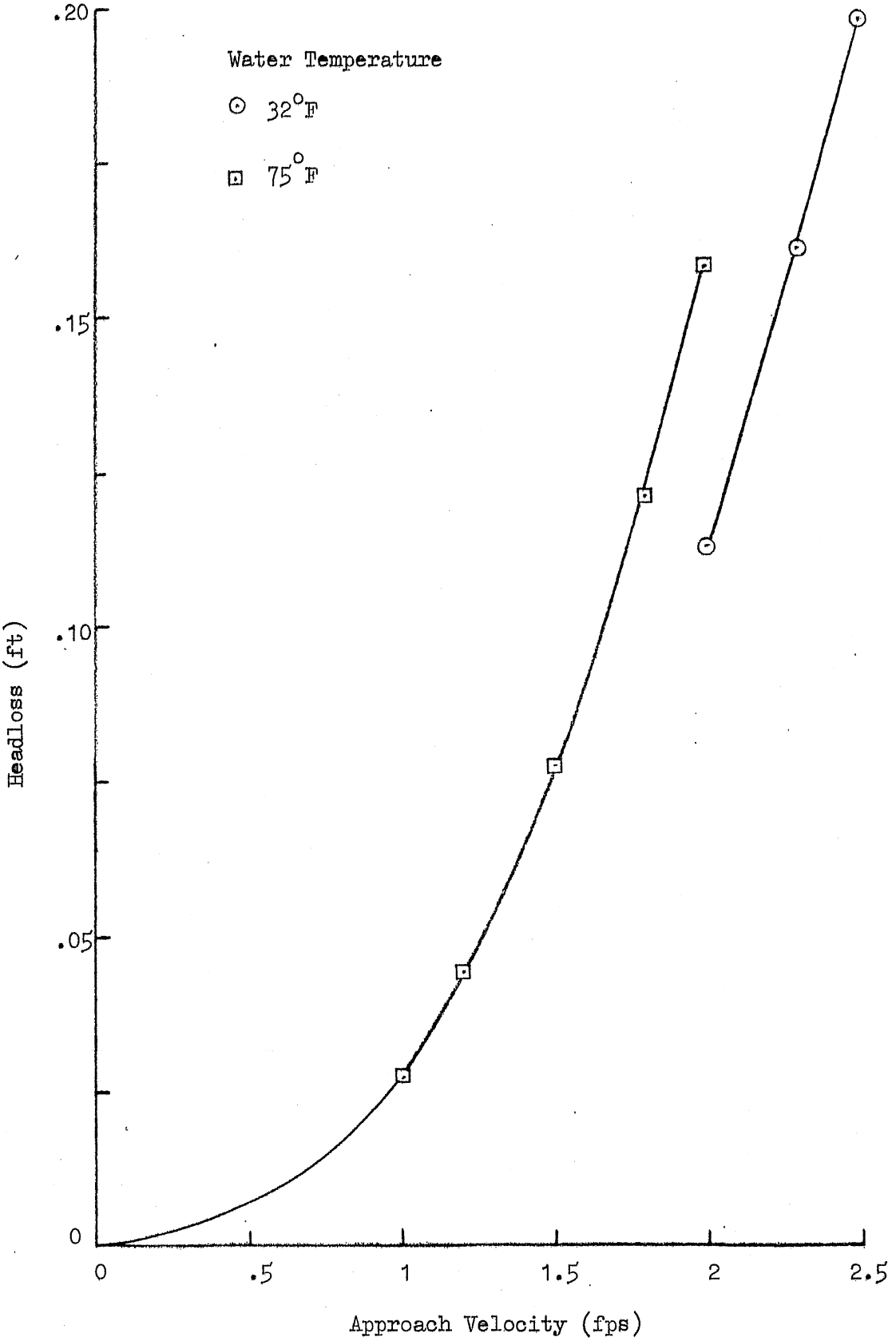

Fig. 22(b) - Headloss of Screen Panel No. 3 (15/16" x 3/8" opening) at Angle of Approach $\beta = 45^{o}$.

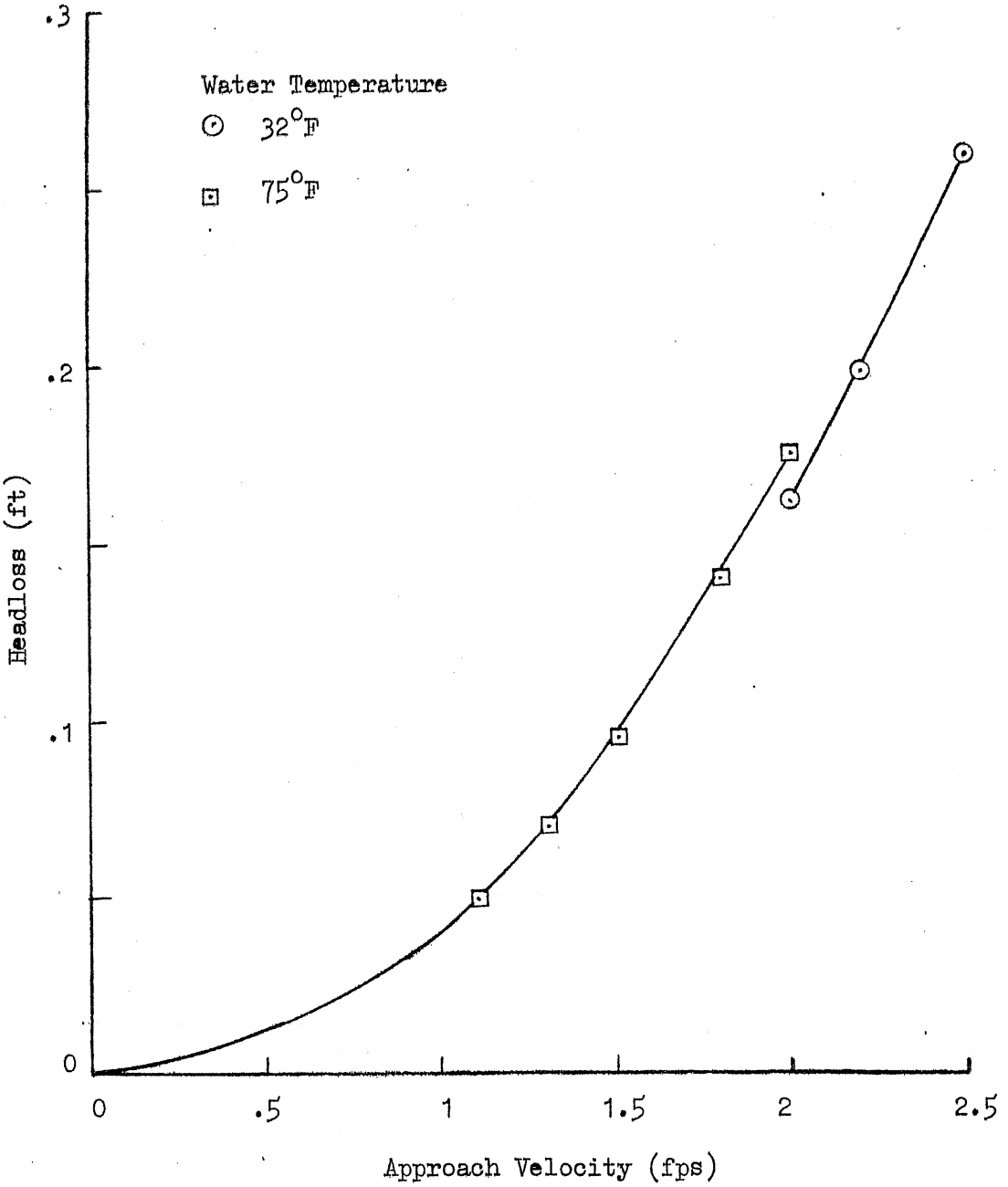

Fig. 22(c) Headloss of Screen Panel No. 4 (3/8" x 3/8" opening) at Angle of Approach $\beta = 45^{\circ}$.

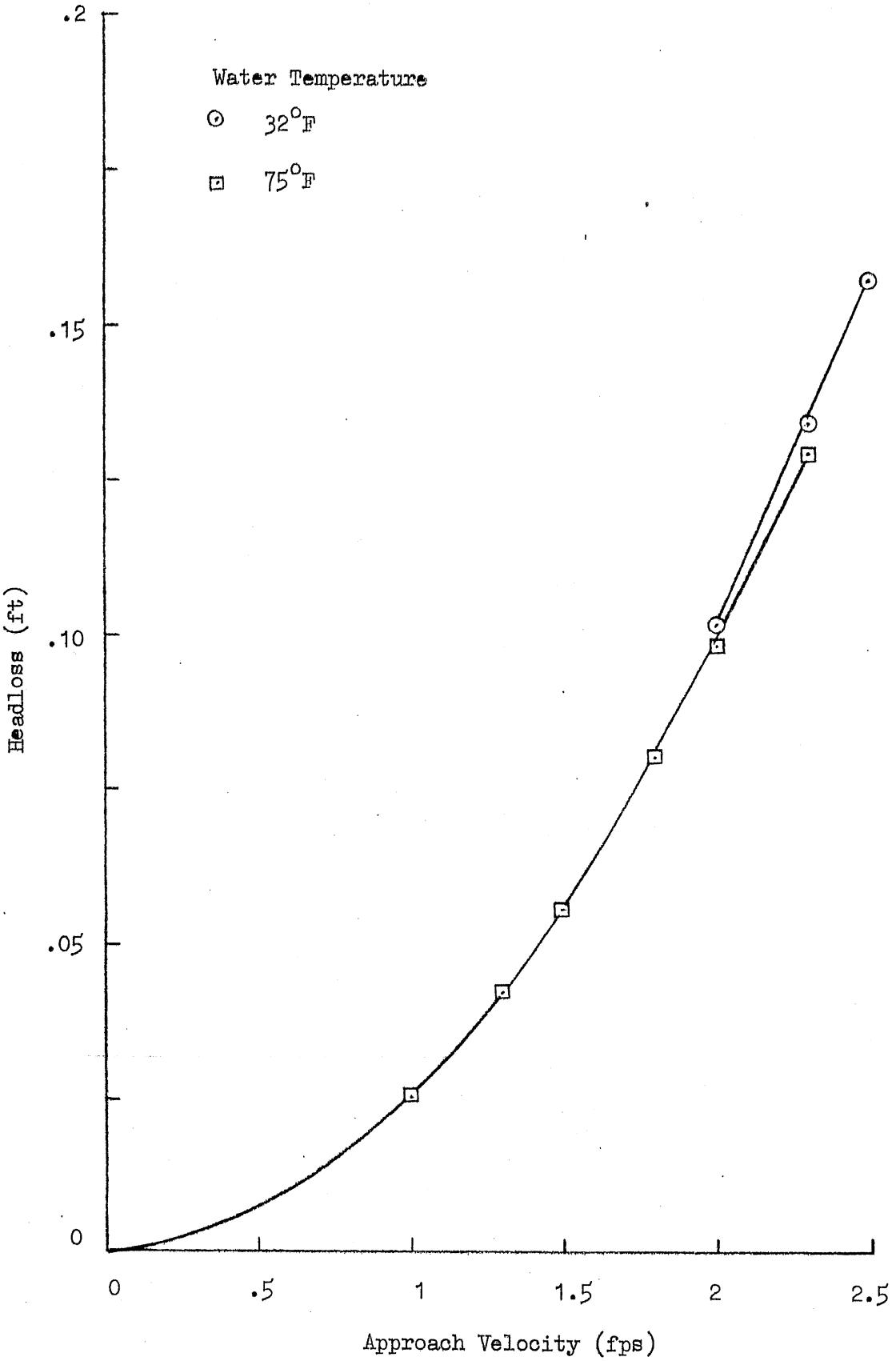

Fig. 22(d) - Headloss of Screen Panel No. 5 (7/8 " x 3/8" opening) at Angle of Approach $\beta = 45^{o}$.

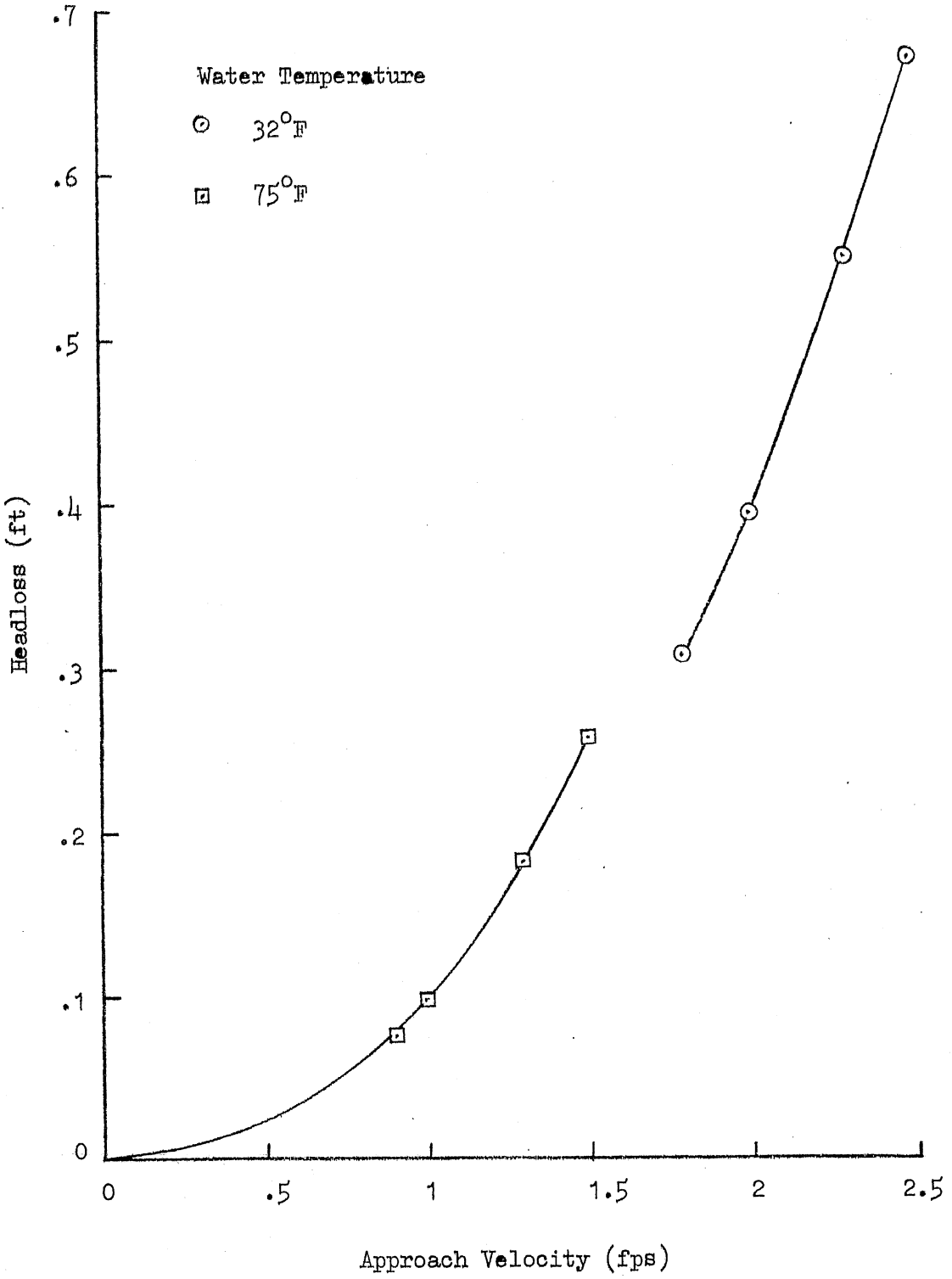

Fig. 22(e) - Headloss of Screen Panel No. 6 (2mm opening) at Angle of Approach $\beta = 45^{\circ}$.

low velocity behind the elements. As the flow passes downstream, the jets and wakes mix to yield finally a uniform flow. Most of the energy loss (headloss) occurs in the mixing process, although some loss also occurs in the flow within the screen passages.

The use of screens in fluid mechanic experimentation to produce turbulence of specific characteristic (grid turbulence) is wide-spread. Eddy scales, frequencies and turbulence intensities are related to screen dimensions and flow Reynolds numbers.

The headloss across a screen is a function of the velocity difference between the jet at the vena contracta and the downstream flow, the geometry of the screen, the viscosity of the fluid, the density of the fluid, and the inclination of screen to the flow direction. Since the bulk of the headloss is due to the interaction of the turbulent shear stress developed at the interface between jets and the ambient fluid, the headloss does not occur right at the screen but over a distance downstream from the screen.

(2) Derivation of Headloss Coefficient in Flow through Screen

Let V_s = velocity at vena contracta of jet

V = upstream or downstream velocity and

a,b,c,e = dimensions of screen elements as defined in Fig. 1

The flow between two wires and that between two rods is depicted in Fig. 23(b) and (c). The flow through a screen opening can be visualized as a combination of (b) and (c) in a three dimensional sense. The flow would be a non-axisymmetric jet. Note that in Fig. 23(c), the velocity at the vena contracta is only approximately equal to V_s. This is because the location of the vena contracta between the wires does not necessarily coincide with that between the rods. Consequently, the following equation of continuity holds approximately true, i.e.

$$V_s \, ab \, C_{cw} \, C_{cr} \approx V(b+c)e \qquad (8)$$

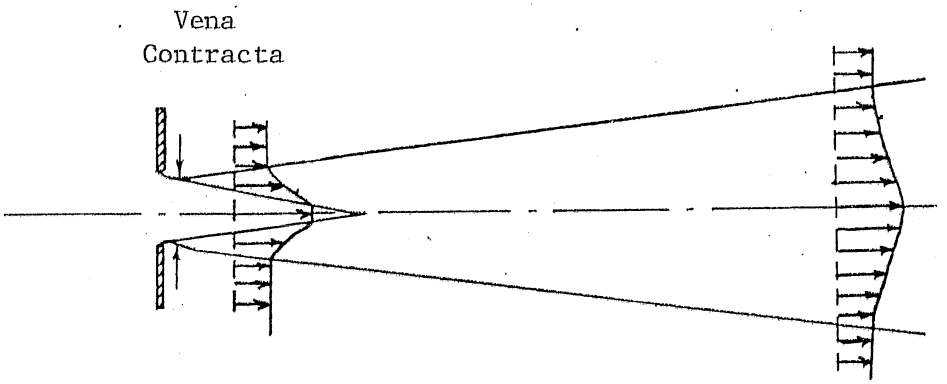

(a) Mean Velocity Distribution in Jet

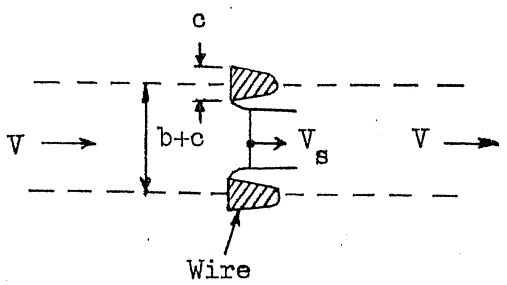

(b) Flow Through Wires

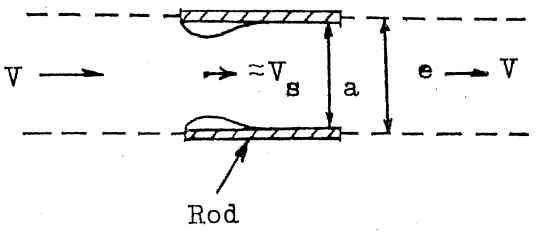

(c) Flow Through Rods

Fig. 23 - Flow Through Single Screen Opening.

where C_{cw} = contraction coefficient of wire

C_{cr} = contraction coefficient of rod

Re-arranging the above equation gives

$$V_s \simeq V \frac{(b+c)e}{abC_{cw}C_{cr}} \tag{9}$$

The headloss (h_L) across the screen is similar to that in an expansion and is given in first approximation by

$$h_L = \frac{(V_s - V)^2}{2g} \tag{10}$$

Substituting Eq. (9) into Eq. (10) gives

$$h_L = \frac{V^2}{2g}\left[\frac{(b+c)e}{abC_{cw}C_{cr}} - 1\right]^2 \tag{11}$$

To account for any Reynolds number effect and for simplifying assumptions, a correction factor η has to be incorporated in Eq. (11). Thus Eq. (11) becomes

$$h_L = \frac{V^2}{2g}\left[\frac{(b+c)e}{abC_{cw}C_{cr}} - 1\right]^2 \eta \tag{12}$$

Expressing the headloss coefficient k as

$$k = \frac{h_L}{V^2/2g} \tag{13}$$

we have, from Eq. (12)

$$k = \frac{h_L}{V^2/2g} = \eta\left[\frac{(b+c)e}{abC_{cw}C_{cr}} - 1\right]^2 \tag{14}$$

(3) Effect of Inclination of Screen

The flow through an inclined screen is illustrated in Fig. 24. The ratio of the obstructed area to the unobstructed flow area remains unchanged. The contraction coefficients, however, have to be modified. Consequently, Eq. (13) can still be applied with a modification of contraction coefficients.

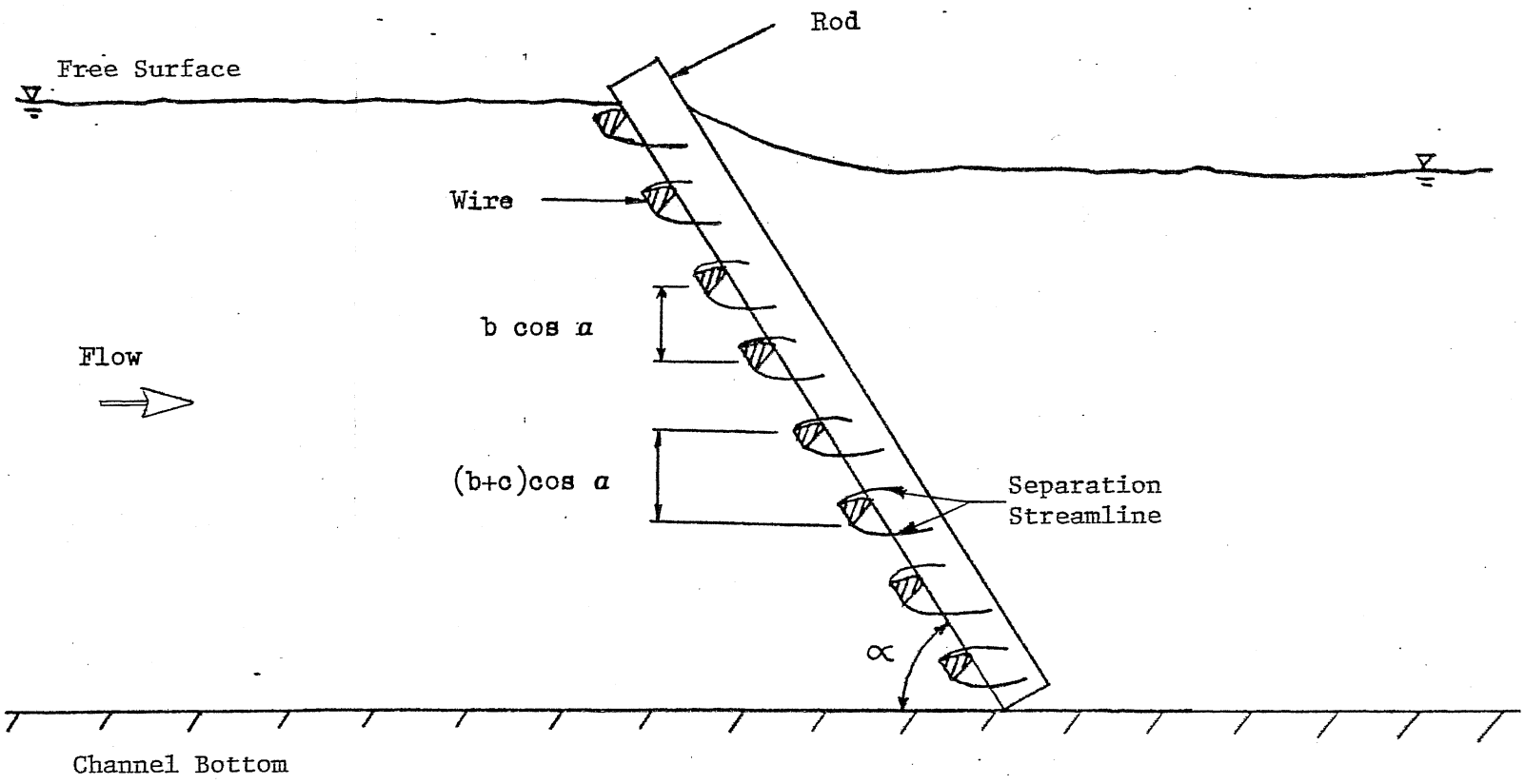

Fig. 24 - Flow Through Inclined Screen - Schematic.

When the screen is inclined at an angle α (as defined in Fig. 4(a) and 4(b)), the contraction coefficient of the wire has to be modified while that of the rods remains unchanged. When the screen is inclined at an angle β (as defined in Fig. 4(c)), the contraction coefficient of the rod has to be modified, while that of the wires remains unchanged.

Values of the contraction coefficients for the wires and rods in the current investigation are not found in the literature. However, values of the contraction coefficients for 2-D sharp edged slots are available (e.g. in Ref. 7). These values can be used to specify the lower limits of the contraction coefficients of the wires and the rods. More accurate estimates of contraction coefficients can be made from experimental headloss data. A tabulation of contraction coefficients, using linear interpolation between values given in Ref. 7 is shown in Tables 2, 3, and 4. It is important to bear in mind that the values in Tables 2, 3, and 4 indicate only the limiting values, and not the actual values of contraction coefficients of the wires and the rods.

(4) Theoretical Headloss Coefficients

Calculation of theoretical headloss coefficients from Eq. 14 requires estimation of η (Reynolds number effect) and the contraction coefficients of wires (C_{cw}) and rods (C_{cr}). The effect of Reynolds number can be determined from experimental data. Exact contraction coefficients C_{cw} and C_{cr} for the screens considered herein cannot be found in the literature. However, lower limits of C_{cw} and C_{cr} can be estimated and have been given in Tables 2, 3, and 4.

As shown in Fig. 10, for $\alpha = 90^{o}$, the contraction coefficients are almost independent of Reynolds number except at low Reynolds numbers.

For $\beta = 60^{o}$, C_{cw} would have the same values as for $\alpha = 90^{o}$. C_{cw}, however, has to be modified. The product $C_{cw}\, C_{cr}$ can be estimated from experimental data with the aid of Eq. 14. Using the known C_{cw} and $C_{cw}\, C_{cr}$, values of C_{cr} can be estimated for different screens.

For $\beta = 75^{o}$ and 60^{o}, C_{cw} would have the same value as for $\alpha = 90^{o}$, as explained earlier. Using the same process as described above, C_{cr} can be estimated for different screens.

TABLE 2

COEFFICIENTS OF JET CONTRACTION AT $\alpha = \beta = 90^\circ$
(By Interpolation from Reference 7)

$\frac{b}{b+c}$ *	$\phi = 45^\circ$	$\phi = 60^\circ$	$\phi = 75^\circ$	$\phi = 90^\circ$	$\phi = 120^\circ$	$\phi = 135^\circ$	$\phi = 150^\circ$	$\phi = 165^\circ$	$\phi = 180^\circ$
0.0	0.746	0.701	0.656	0.611	0.562	0.537	0.525	0.513	0.500
0.1	0.747	0.702	0.657	0.612	0.568	0.546	0.535	0.524	0.513
0.2	0.747	0.703	0.660	0.616	0.575	0.555	0.546	0.537	0.528
0.3	0.748	0.706	0.664	0.622	0.585	0.566	0.559	0.552	0.544
0.4	0.749	0.710	0.671	0.631	0.597	0.580	0.575	0.570	0.564
0.5	0.752	0.716	0.680	0.644	0.614	0.599	0.595	0.591	0.586
0.6	0.758	0.726	0.694	0.662	0.634	0.620	0.618	0.616	0.613
0.7	0.768	0.741	0.714	0.687	0.664	0.652	0.650	0.648	0.646
0.8	0.789	0.767	0.745	0.722	0.706	0.698	0.696	0.694	0.691
0.9	0.829	0.813	0.797	0.781	0.768	0.761	0.761	0.761	0.760
1.0	1.000	1.000	1.000	1.000	1.000	1.000	1.000	1.000	1.000

* See Fig. 1 for definition.

Definition sketch for slots 2-D

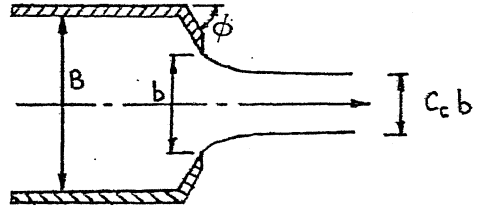

TABLE 3

Coefficients of Jet Contraction for Rods

a/e*	$\beta = 75^\circ$ mean of(165°, 75°)	$\beta = 60^\circ$ mean of(60°, 150°)	$\beta = 45^\circ$ mean of(45°, 135°)
0.0	0.58	0.61	0.64
0.1	0.59	0.62	0.65
0.2	0.60	0.62	0.65
0.3	0.61	0.63	0.66
0.4	0.62	0.64	0.67
0.5	0.64	0.65	0.68
0.6	0.65	0.67	0.69
0.7	0.68	0.70	0.71
0.8	0.72	0.73	0.74
0.9	0.78	0.79	0.80
1.0	1.00	1.00	1.00

Angle β defined in Fig. 4(c).

*See Fig. 1 for definition.

TABLE 4

Coefficients of Jet Contraction

for Wire

$\frac{b}{b+a}$ *	$\alpha = 60^\circ$ mean of $(60^\circ, 120^\circ)$	$\alpha = 45^\circ$ mean of $(45^\circ, 135^\circ)$
0.0	0.63	0.64
0.1	0.63	0.65
0.2	0.64	0.65
0.3	0.65	0.66
0.4	0.65	0.67
0.5	0.67	0.68
0.6	0.68	0.69
0.7	0.70	0.71
0.8	0.74	0.74
0.9	0.79	0.80
1.0	1.00	1.00

a defined in Fig. 4(b).

* See Fig. 1 for definition.

Headloss coefficients calculated from the estimated contraction coefficients are shown in Tables 5 through 8.

Theoretical prediction of headloss coefficients hinges essentially on proper estimates of contraction coefficients. Such estimates are difficult when separation points are not clearly identified, as in the case for round-wire screens. Equation (14) is very sensitive with respect to contraction coefficients. In addition to jet dissipation losses, wall friction of the screen elements can make an important contribution to headlosses at very low Reynolds number.

IX. Headlosses at Low Approach Flow Velocities

The experimental screen headloss data reported in Section VII were obtained at approach flow velocities from 0.9 to 2.6 ft/sec. The maximum through-screen design velocity for the Campbell intake is 0.5 ft/sec. The purpose of the headloss measurements in the laboratory was to determine whether screen losses were significant when compared to other losses, specifically those in the risers and headers. Very early in the experiments it was found that at velocities of 0.5 ft/sec and less, the screen losses could not be measured in the channel without resorting to micromanometry. Therefore, higher approach flow velocities were used.

In the experimental flume the approach flow was always turbulent. The flow around the wires and rods was a separated flow producing a wake downstream from each rod or wire. Had the velocities been decreased separation would have become less pronounced as is well known from the fundamentals of fluid mechanics. At extremely low velocity the flow would have even remained attached. It is well known that in the case of a cylinder complete attachment of the flow requires a cylinder Reynolds number on the order of about 1.0. That Reynolds number is defined as VD/ν, where V is the approach flow velocity, D is the cylinder diameter and ν is the kinematic viscosity. The Reynolds numbers for the flow around the wires and rods of a Johnson screen at through-screen velocities from 0.1 to 0.5 ft/sec would be on the order of 25 to 500, well above the range of fully attached flows. The flow regime through a Johnson screen in the velocity range from 0.1 to 0.5 ft/sec can therefore be

TABLE 5. Theoretical Headloss Coefficient of Screen Panels at $\alpha = 90^{o}$ (without Reynolds number effect).

Screen No.	a (in)	b (in)	c (in)	e (in)	$\frac{b}{b+c}$	$\frac{a}{e}$	Estimated Values C_{cw}	C_{cr}	$k' = \left[\frac{e(b+c)}{ab\ C_{cw}\ C_{cr}} - 1\right]^2$
1	0.930	3/8	0.128	1	0.746	0.930	0.85	0.92	0.7
2	0.930	1/2	0.128	1	0.796	0.930	0.85	0.92	0.5
3	0.930	3/8	0.128	1	0.746	0.930	0.85	0.92	0.7
4	0.348	3/8	0.128	0.5	0.746	0.696	0.95	1.00	1.0
5	0.848	3/8	0.128	1	0.746	0.848	0.85	1.00	0.7
6	0.930	2mm	0.075	1	0.513	0.930	0.80	0.92	2.8

TABLE 6. Theoretical Headloss Coefficients of Screen Panels at $\alpha = 60^{\circ}$ (without Reynolds number effect)

Screen No.	a (in)	b (in)	c (in)	e (in)	$\frac{b}{b+c}$	$\frac{a}{e}$	Estimated Values C_{cw}	Estimated Values C_{cr}	$k' = \left[\frac{e(b+c)}{ab\ C_{cw}\ C_{cr}} - 1\right]^2$
1	0.930	3/8	0.128	1	0.746	0.930	0.75	0.92	1.2
3	0.930	3/8	0.128	1	0.746	0.930	0.75	0.92	1.2
4	0.348	3/8	0.128	0.5	0.746	0.696	0.85	1.00	1.6
5	0.848	3/8	0.128	1	0.746	0.848	0.75	1.00	1.2
6	0.930	2mm	0.075	1	0.513	0.930	0.78	0.92	3.7

TABLE 7. Theoretical Headloss Coefficients of Screen Panels at $\beta = 75^{\circ}$ (without Reynolds number effect.

Screen No.	a (in)	b (in)	c (in)	e (in)	$\frac{b}{b+c}$	$\frac{a}{e}$	Estimated Values C_{cw}	Estimated Values C_{cr}	$k' = \left[\frac{e(b+c)}{ab\ C_{cw}\ C_{cr}} - 1\right]^2$
1	0.930	3/8	0.128	1	0.746	0.930	0.85	0.90	0.8
3	0.930	3/8	0.128	1	0.746	0.930	0.85	0.90	0.8
4	0.348	3/8	0.128	0.5	0.746	0.696	0.95	1.00	1.1
5	0.848	3/8	0.128	1	0.746	0.848	0.85	1.00	0.7

TABLE 8. Theoretical Headloss Coefficients of Screen Panels at $\beta = 60^{\circ}$ (without Reynolds number effect).

Screen No.	a (in)	b (in)	c (in)	e (in)	$\frac{b}{b+c}$	$\frac{a}{e}$	Estimated Values C_{cw}	Estimated Values C_{cr}	$k' = \left[\frac{e(b+c)}{ab\ C_{cw}\ C_{cr}} - 1\right]^2$
1	0.930	3/8	0.128	1	0.746	0.930	0.85	0.85	1.0
3	0.930	3/8	0.128	1	0.746	0.930	0.85	0.85	1.0
4	0.348	3/8	0.128	0.5	0.746	0.696	0.95	0.95	1.3
5	0.848	3/8	0.128	1	0.746	0.848	0.85	0.95	0.9

expected to be in the transition range between fully attached and fully turbulent. In that range the headloss coefficients are likely to vary with Reynolds number. An indication of such variations is already shown in Figs. 9 through 15. As the Reynolds numbers in those figures are lowered by a factor of two or more, the variations are likely to continue.

Headlosses through the Johnson screens at low approach flow velocities are small. For comparison with other losses in the Campbell intake system an upper bound for the screen headlosses can be specified using Figs. 16 through 22. Since the maximum through-screen velocity is 0.5 ft/sec, headloss bounds will be given for that velocity only. The approach flow velocity will be calculated by multiplication of the through-screen velocity (0.5 ft/sec) with the open area percentage given in Table 1. The upper bound of the headloss will be estimated as the arithmetic mean of the following two values; one determined from the curve shown on Figs. 16 through 22(b) and the other read on a straight-line connection from the origin of each graph to the nearest data point. Each value is read at the approach flow velocity shown in Table 9. The first reading is the best graphical extrapolation from the given data, and the second reading would be obtained if the flow were fully laminar between zero velocity and the last data point.

X. Conclusions

Headlosses experienced by the flow of water through six Johnson screens of different geometries (see Table 1 and Figs. 1 and 2) have been measured and analyzed. Measurements were made at approach flow velocities from 0.9 to 2.5 ft/sec. The measurements were made in a 24 inch wide laboratory channel. The screens were placed at angles of 90°, 75°, 60° and 45° relative to the channel axis. The objective of the experiments was to establish the order of magnitude of the headloss to determine if it could be ignored in the design of the James H. Campbell cooling water intake risers. The flow rates in the channel were varied to change the approach flow velocity.

The headloss data were reduced to headloss coefficients, using the approach flow velocity head as a reference and plotted versus a mesh Reynolds

TABLE 9

Upper Bound for Screen Headloss at a Through-Screen Velocity of 0.5 ft/sec at 75°F Water Temperature

Panel No.	Opening Ratio (%)	Approach Velocity (ft/sec)	Orientation α	Orientation β	Upper Bound Headloss (ft)
1,3,5	74.5	.37	90°	90°	.002
4	74.5	.37	90°	90°	.003
6	51.3	.26	90°	90°	.008
6	51.3	.26	75°	90°	.008
1,3,5	74.5	.37	60°	90°	.004
4	74.5	.37	60°	90°	.006
6	51.3	.26	60°	90°	.008
1,3,5	74.5	.37	45°	90°	.006
4	74.5	.37	45°	90°	.008
6	51.3	.26	45°	90°	.008
1	74.5	.37	90°	75°	.003
3,5	74.5	.37	90°	75°	.003
4	74.5	.37	90°	75°	.004
1	74.5	.37	90°	60°	.006
3	74.5	.37	90°	60°	.005
4	74.5	.37	90°	60°	.005
5	74.5	.37	90°	60°	.004
1	74.5	.37	90°	45°	.016
3	74.5	.37	90°	45°	.008
4	74.5	.37	90°	45°	.013
5	74.5	.37	90°	45°	.007
6	51.3	.26	90°	45°	.015

number (Figs. 9a through 15). The dependence of the coefficients on Reynolds number in the data range is not very strong. The coefficients tend to decrease somewhat as the Reynolds numbers are lowered suggesting that the flow regime through the screen may be in the transition to fully develop turbulent flow. The trend of lowered headloss coefficients at lower Reynolds numbers is consistent for all angles of α investigated, (α is the angle between the channel bottom and the screen faces, see Fig. 4), but not for all angles of β (β is the angle between the channel wall and the screen face, see Fig. 4).

When β is less than 90° it was observed that the flow is deflected by the rods and reoriented towards the channel wall. The resulting impact (momentum loss) probably affects the measured headloss. It appears also that at $\beta = 60^{\circ}$, the effect of flow concentration between wires becomes less important than the length of the rod in determining the headloss.

Because the design flow velocity in the James H. Campbell cooling water intake is much less than the velocity used in the experiments described herein, a set of charts was prepared (Figs. 16a through 22e) in which headloss is plotted versus approach flow velocity for water temperatures of 32°F and 75°F. Between the last data point and the origin (zero headloss at zero velocity) the curves are interpolated. These graphs show that at low approach flow velocities the headloss through the Johnson screens is very small. Upper limits for screen headloss at 0.5 ft/sec through screen velocity have been estimated in Table 9. Summarizing the results in Table 9, it can be stated that at 0.5 ft/sec through-screen velocity and at angles of approach from 60° to 90° (for both α or β) the headloss through a clean screen will not exceed 0.008 ft or one-tenth of an inch of water for all six screens investigated, including one with a 2 mm opening between wires. At an angle of approach of 45° it could be up to two-tenths of an inch of water. It should be pointed out, however, that the measurements at $\beta = 45^{\circ}$ screen inclination are probably the least reliable because of the wall effects in the laboratory flume.

A comparison of the experimental results with separated flow theory over blunt objects shows that headloss coefficients increased as open area fraction of the screen decreased, pretty much as predicted by theory. Purely theoretical headloss prediction for screens is, however, not advisable because it requires very precise estimates of flow contraction coefficients. Such coefficients are usually not available in the literature for the

variety of geometrical configurations and flow conditions encountered for commercial screens.

All results presented are for clean screens only. Debris accumulated on a screen panel was removed prior to every measurement.

REFERENCES

(1) Chemical Engineers Handbook, Section 5, by John Perry, Robert H. Perry, Cecil H. Chilton, and Sidney D. Kirkpatrick, McGraw-Hill Book Co., Inc., 1963.

(2) Handbook of Hydraulic Resistance, Coefficients of Local Resistance and of Friction, Section 8, by I. E. Idel'Chik, translation from Russian. Published for the U.S. Atomic Energy Commission and the National Science Foundation, available from National Technical Information Service, AEC-TR-6630.

(3) Internal Flow: A Guide to Losses in Pipe and Duct Systems, by Donald S. Miller, published by British Hydromechanics Research Association, Cranfield, Bedford, England, 1971, 329 pp.

(4) MacDougall, "Loss Coefficients of Duct Geometries, Nozzles, Orifices, Perforations, Grids, and Screens", Program 5014, Project 1-2104A, Donaldson Co., Inc., Dec. 1974.

(5) Cornell, W. G., "Losses in Flow Normal to Plane Screens", Transactions of the American Society of Mechanical Engineers, Vol. 80, May 1978, pp. 791-799.

(6) Wieghardt, K. E. G., "On the Resistance of Screens", The Aeronautical Quarterly, Vol. 4, Feb. 1953, pp. 186-192.

(7) Engineering Hydraulics, Chapt. I, Section C, edited by H. Rouse, John Wiley and Sons, 1949, 1039 pp.